



Article

Future Projections of Extreme Precipitation Climate Indices over South America Based on CORDEX-CORE Multimodel Ensemble

Michelle Simões Reboita ^{1,2,*}, Rosmeri Porfírio da Rocha ³ , Christie André de Souza ¹, Thales Chile Baldoni ¹, Pedro Lucas Lopes da Silveira Silva ¹ and Glauber Willian S. Ferreira ¹

¹ Instituto de Recursos Naturais, Universidade Federal de Itajubá—UNIFEI, Itajubá 37500-093, Brazil

² The Abdus Salam International Centre for Theoretical Physics—ICTP, 34151 Trieste, Italy

³ Departamento de Ciências Atmosféricas, Universidade de São Paulo—USP, São Paulo 05508-090, Brazil

* Correspondence: reboita@unifei.edu.br

Abstract: Climate change is undeniable, and its effects, like droughts and intense precipitation, evidence this reality. However, many questions remain unanswered, such as climate extremes' future frequency and intensity. International collaboration projects such as the Coordinated Regional Climate Downscaling Experiment (CORDEX)-Coordinated Output for Regional Evaluations (CORE) have emerged to address these questions, creating protocols to facilitate the intercomparison among simulations obtained by different regional climate models (RCMs). Given this context, this study aims to describe the projected changes in the extreme precipitation events over the South America domain by using a set of projections of three RCMs (Eta, RegCM, and REMO) under the CORDEX-CORE framework (except Eta). These models were nested in different global climate models (GCMs) from Coupled Model Intercomparison Project phase 5 (CMIP5) under the RCP8.5 scenario and integrated with a grid space of 25 km. In addition, six climate indices (PRCPTOT, SDII, R95p, P95, CDD, and CWD) were computed by season for the historical period (1995–2014) and four future time-slices (2020–2039, 2040–2059, 2060–2079, and 2080–2099). For brevity, this study focuses on the austral summer. RCMs are generally capable of representing the spatial pattern of climate indices but with differences in intensity. The ensemble with all RCMs shows a slightly better spatial correlation with the reference data than the ensemble of each RCM. The signal of the projections is similar between RegCM and REMO and, in general, opposite to Eta (mainly in the South Atlantic Convergence Zone region). Of the six climate indices analyzed, the ensemble performed with the three RCMs projects statistically significant negative (positive) trends for four indices in the Amazon (La Plata Basin), indicating a signal of dry (wet) conditions increasing towards the end of the century. Furthermore, both regions have significant positive (negative) trends of consecutive dry (wet) days. The region with higher uncertainties lies over southeastern Brazil, where Eta projects a dry climate and RegCM and REMO, a wet one.

Keywords: CORDEX-CORE; South America; climate projections; precipitation climate indices; trends; uncertainties



Citation: Reboita, M.S.; da Rocha, R.P.; Souza, C.A.d.; Baldoni, T.C.; Silva, P.L.L.d.S.; Ferreira, G.W.S. Future Projections of Extreme Precipitation Climate Indices over South America Based on CORDEX-CORE Multimodel Ensemble. *Atmosphere* **2022**, *13*, 1463. <https://doi.org/10.3390/atmos13091463>

Academic Editors: Jason C. Knievel and Stefano Federico

Received: 23 July 2022

Accepted: 7 September 2022

Published: 9 September 2022

Publisher's Note: MDPI stays neutral with regard to jurisdictional claims in published maps and institutional affiliations.



Copyright: © 2022 by the authors. Licensee MDPI, Basel, Switzerland. This article is an open access article distributed under the terms and conditions of the Creative Commons Attribution (CC BY) license (<https://creativecommons.org/licenses/by/4.0/>).

1. Introduction

As we already feel the effects of climate change, there is no doubt whether it indeed exists [1–3]. On the other hand, many questions remain regarding the climate system's characteristics in the future [2,4–8]. To contribute to the knowledge of the future climate, different climate modeling groups have run numerical models and made the simulations/projections available to researchers across the globe. However, it is a coordinated task under the efforts of the World Climate Research Program (WCRP).

Climate projections can be obtained from global climate models (GCMs) and regional climate models (RCMs). While GCMs need only initial conditions to simulate the atmo-

spheric conditions around the globe, RCMs simulate limited areas and are time-dependent on the lateral boundary conditions, i.e., the outputs of GCMs [9]. Thus, the path of climate change studies begins with GCMs. The Coupled Model Intercomparison Project (CMIP) [10] of WCRP (<https://www.wcrp-climate.org/wgcm-cmip>, accessed on 15 July 2022), among its several aims, has the responsibility of creating protocols to guide GCMs researcher groups and allow the projections comparisons. Projections of different CMIP phases are freely available on Earth System Grid Federation (ESGF) platform (<https://esgf.llnl.gov/>, accessed on 15 July 2022).

RCMs also have a WCRP group for designing the projections protocols, the Coordinated Regional Climate Downscaling Experiment (CORDEX) [11,12]. The first set of CORDEX projections was performed with 50 km of horizontal resolution [13], and these projections provided information for the Fifth Assessment Report (AR5) of the Intergovernmental Panel on Climate Change (IPCC). However, concerning the newest IPCC report, AR6 [2], the CMIP phase 6 (CMIP6) provided the GCMs' projections, but the GCMs from CMIP5 drove the RCMs for the AR6. This procedure was due to RCMs consuming a long processing time, and waiting for CMIP6 GCMs' availability to run RCMs would delay the AR6-IPCC release. Hence, RCMs driven by the CMIP5 GCMs and run with 25 km of horizontal resolution compounded the second phase of CORDEX, called CORDEX Coordinated Output for Regional Evaluations (CORDEX-CORE) [14].

Regional Climate Model version 4 (RegCM4) [15] from the International Centre for Theoretical Physics (ICTP), and REMO version 2015 (REMO2015) [16] from the Climate Service Center Germany (GERICS), were the RCMs used in the CORDEX-CORE experiments. These models were run for different CORDEX domains, including the South America domain (SAM). Moreover, from an independent initiative [17], Eta model was also run for SAM at the Instituto Nacional de Pesquisas Espaciais (INPE) in Brazil. Each RCM was nested in three different CMIP5-GCMs (see Section 2), and their projections are also available on the CORDEX-ESGF platform (<https://cordex.org/data-access/esgf/>, accessed on 15 July 2022).

For SAM, it is common to find in the literature studies addressing only one of the mentioned RCMs, whether to evaluate the historical period or to analyze projections [16–22], while those focusing on the ensemble mean of the three RCMs are scarcer [23–28]. For example, considering the CORDEX phase 1, Falco et al. [23] and Solman and Blázquez [24] evaluated the added value of different RCMs regarding their GCMs drivers in the historical simulations. Falco et al. [23] included in their analyses five models (and, among them, were RegCM and REMO), and Solman and Blázquez [24] analyzed three models, among them REMO. On the other hand, Llopert et al. [25] and Spinoni et al. [26] also addressed future scenarios using RegCM, REMO, and RCA.

Recently, for CORDEX phase 2, the Climate Dynamics journal published a special issue for the CORDEX-CORE Experiment [14]. Seven papers analyzed the SAM domain [28–34], but very few of them focused on both RegCM4 and REMO. In addition, no study calculated and evaluated climate indices, which are a tool for studying extreme climate. Teichmann et al. [28] is one study example of this special issue focusing on both RegCM4 and REMO performance over different CORDEX domains. Olmo and Bettolli [27], not included in the special issue, also evaluated the performance of different RCMs over southern South America (SA). Amongst the studies addressing only one RCM, we can mention Remedio et al. [17], which assessed the quality of the simulated climate and its fitness for climate change projections by REMO2015, including a study of Köppen–Trewartha (K–T) Climate Classification types. Dereczynski et al. [21] evaluated the temperature and precipitation trends simulated for the present climate by the Eta model driven by three GCMs. The temperature simulations of the Eta-CanESM2 (Eta-MIROC5) showed the largest (smallest) trends among the three simulations. For precipitation, Eta-MIROC5 presented a better performance. Reboita et al. [20] computed 19 climate indices with Eta projections under the Representative Concentration Pathway (RCP) 4.5 and 8.5 scenarios for SAM. According to the authors, the climate change signal for the 19 climate indices is more intense under

RCP8.5, and the regions more susceptible to climate change are the Amazon, northeastern Brazil, and southeastern SA. Ashfaq et al. [29] and Teodoro et al. [22] studied the features of the South American Monsoon in the present and future climate using RegCM4 ensembles. One result is that the region defined as the monsoon in the present climate does not show significant shrinkage or expansion in the future climate.

One way to know the extreme events changes in the climate is through climate indices [35]. For this purpose, the CCI/CLIVAR/JCOMM Expert Team (ET) on Climate Change Detection and Indices (ETCCDI) [36,37] has developed 27 climate indices to help the characterization of climate variability and climate changes (the indices description is provided at http://etccdi.pacificclimate.org/list_27_indices.shtml, accessed on 15 July 2022). These indices allow the intercomparison of the extreme events obtained with different datasets and in distinct regions of the globe [38]. For SAM, Reboita et al. [20] reported that many studies are available using the ETCCDI indices for the present climate, but the same does not occur for the future climate. The authors also highlight that few studies address the features of extreme events by season and consider the whole South American continent under climate scenarios. Here we add another literature gap: The scarcity of studies addressing the climate indices by an ensemble mean with the CORDEX-CORE projections.

Based on the previous review, this study aims to use the CORDEX-CORE RCMs (RegCM4 and REMO2015) and Eta nested in different GCMs from CMIP5 under the RCP8.5 scenario to calculate and analyze a selection of ETCCDI indices for extreme events of precipitation over SAM domain. Moreover, our second goal is to provide an interactive atlas with the obtained results. The scientific questions we want to answer are: how is the projection of the seasonal volumes of precipitation (PRCPTOT) under the RCP8.5 scenario and the intensity of the precipitation during wet days (SDII)? What are the regions with increases in the frequency (R95p) and/or intensity (P95) of the extreme daily precipitation? How are the sequence of consecutive dry (CDD) and wet (CWD) days per season projected to change? These indices were selected because they answer questions frequently asked by decision-makers and administrators in the energy sector. As for the latter, there is an enormous concern, given that South America's energy matrix is primarily hydroelectric, accounting for 48% of the region's energy generation [39]. Within this framework, Brazil leads with 55% of the hydropower produced in Latin America [40] and is also the second largest producer worldwide, behind only China [41]. Given the background, this work will focus on the wettest period of SA, which is December-January-February (DJF), but a complete seasonal analysis is provided in the interactive atlas at https://meteorologia.unifei.edu.br/south_america_climate_projection/CORDEX_ClimateIndices, accessed on 15 July 2022. This study is in line with WCRP (wcrp-climate.org, accessed on 15 July 2022) and CORDEX project and will be a source of valuable information for stakeholders.

2. Materials and Methods

2.1. Study Area

The study area is SA (Figure 1), which extends from 55° S to 12° N and covers areas in different climate zones (extratropical, subtropical, and tropical) [42,43]. However, most SA is characterized by a monsoon climate, i.e., well-defined wet and dry seasons. The wet season occurs from October to March, with the peak in December-January-February (DJF), and the dry season extends from April to September [22,29,43]. Furthermore, two hydrological basins with global importance are located in SA: the Amazon basin, located in northern SA, is the largest drainage basin in the world, and the La Plata basin, located in the southeastern part of the continent, is in the sixth position [44]. Therefore, this study will also focus on these two hydrological basins (Figure 1).

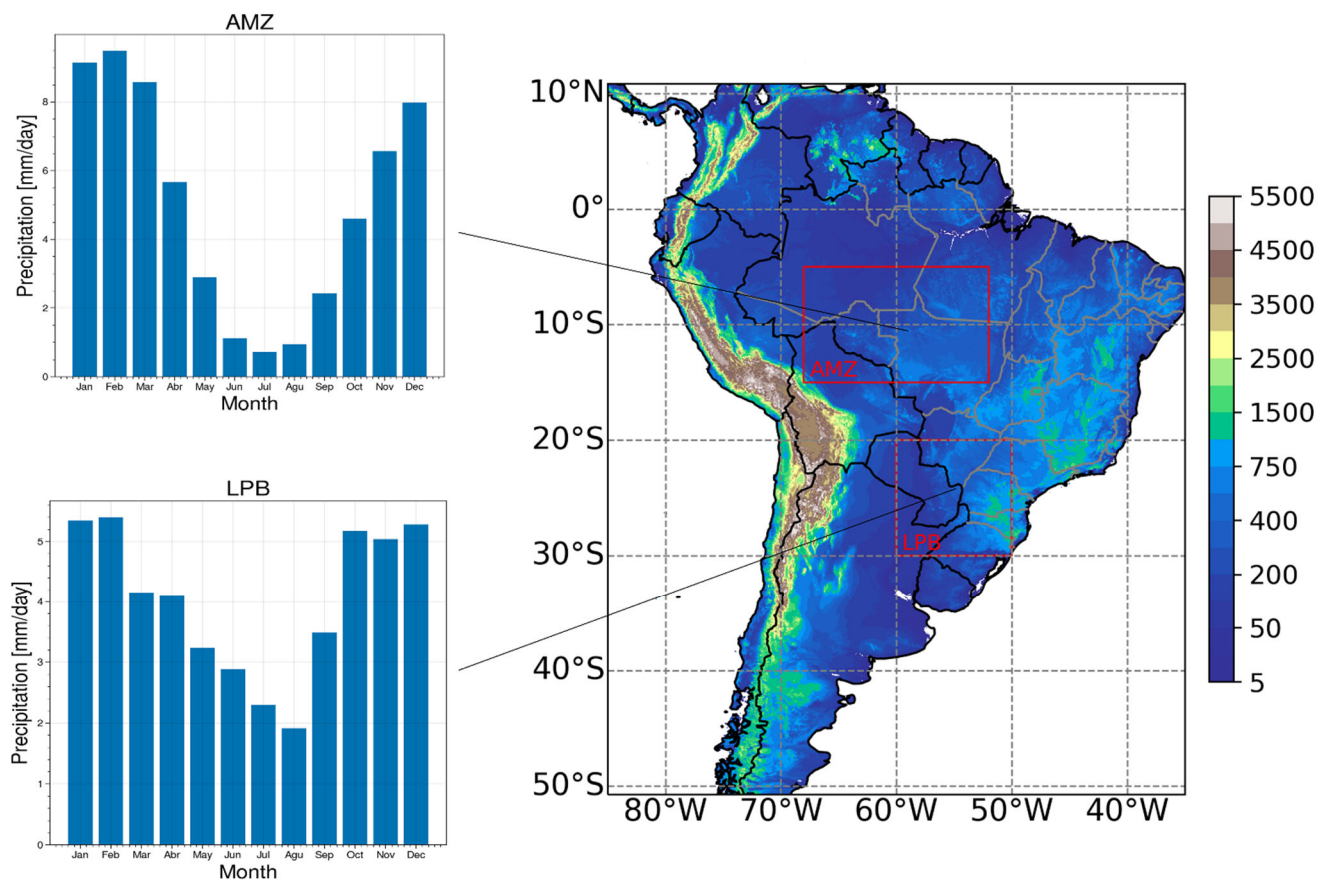


Figure 1. Study area (with topography in meters) and the subdomains (red boxes) located at the main hydrological basins—the Amazon and La Plata basins—with the annual mean cycle of precipitation (1995–2014) obtained from CPC. Topography source: United States Geological Survey—Earth Resources Observation System (EROS) Center.

2.2. Data

Daily precipitation (mm/day) of the Climate Prediction Center (CPC) [45] from 1995 to 2014 is used. These data cover the globe with 0.5° of horizontal resolution and are generated through the optimal interpolation (OI) objective analysis technique of precipitation measured in situ. The grid dataset is freely available at <https://psl.noaa.gov/data/gridded/data.cpc.globalprecip.html>, accessed on 15 July 2022. In addition, CPC has been used as a reference dataset in different studies such as Marrafon and Reboita [46], Blázquez and Solman [47], and Balmaceda-Huarte et al. [48].

2.3. RCM Projections

Climate projections from two RCMs (RegCM4 and REMO2015, hereafter RegCM and REMO) of the CORDEX-CORE framework and the Eta model (Table 1) are analyzed over the SAM domain (this acronym is defined by CORDEX). These simulations were obtained from the CORDEX-ESGF platform. All RCMs use roughly the same domain and horizontal resolution ($\sim 0.22^\circ \times \sim 0.22^\circ$ or $25 \times 25 \text{ km}^2$) following the CORDEX recommendations. The simulation period is from 1970 to 2100 (except for Eta, which begins in 1960), with the Representative Concentration Pathways (RCPs) [49] scenarios starting in 2006. Following the IPCC recommendation for AR6, we consider the reference period 1995–2014 (hereafter the historical period). The current global warming has already exceeded the warming projected by RCP2.6 [50,51], and WMO [50] reported that “2019 was already 1.1°C warmer than the pre-industrial era”. So, although the CORDEX-CORE models were run for the scenarios RCP2.6 and RCP8.5, our focus here is only on RCP8.5, a more pessimistic scenario.

To compare the historical period of the RCMs with the reference dataset, we interpolated all original simulations onto the CPC regularly spaced latitude/longitude grid using a bilinear interpolation procedure. In this study, we did not include the driving GCMs since previous studies showed better performance of RCMs in representing the SA climate in the historical period than their drivers [20,23,24,28,47]. For example, Solman and Blázquez [24], comparing various CMIP5-GCMs (some of them used in the present study) and CORDEX-phase1 RCMs over SA, showed that RCMs added value to driven GCMs in several temporal scales, mainly for smaller scales including the extreme rainfall events. Moreover, in the Climate Indices Atlas from Reboita et al. [20], the authors calculated the climate indices per season for the GCMs (the same models of the present study) that drove the Eta model (https://meteorologia.unifei.edu.br/projacao_climatica/, accessed on 15 July 2022). Therefore, the GCMs suppression here avoids results repetition from previous literature.

Table 1. Specification of RCMs and their driven GCMs.

RCM	Horizontal Resolution and Reference	GCM	GCM Resolution	References
Eta	0.20° × 0.20°	CanESM2	2.7906° × 2.8125°	Chylek et al. [53]
	Mesinger et al. [52]	HadGEM2-ES	1.25° × 1.875°	Arora et al. [54]
	Chou et al. [17]	MIROC5	1.4008° × 1.40625°	Collins et al. [55] Martin et al. [56] Watanabe et al. [57]
RegCM4	0.22° × 0.22°	HadGEM2-ES	1.25° × 1.85°	Collins et al. [55]
	Giorgi et al. [14]	NorESM1-M	1.8947° × 2.5°	Martin et al. [56]
		MPI-ESM-MR	1.8653° × 1.875°	Bentsen et al. [58] Stevens et al. [59]
REMO2015	0.22° × 0.22°	HadGEM2-ES	1.25° × 1.875°	Collins et al. [55]
	Jacob et al. [60]	NorESM1-M	1.8947° × 2.5°	Martin et al. [56]
	Remedio et al. [16]	MPI-ESM-LR	1.8653° × 1.875°	Bentsen et al. [58] Stevens et al. [59]

2.4. Climate Indices

This study calculates six climate indices (PRCPTOT, SDII, P95, R95p, CDD, and CWD; Table 2) defined by ETCCDI [36,37]. These indices are based on daily precipitation amounts and are calculated at each grid point and season. While PRCPTOT is an index used to describe the mean state of the climate, R95p and CDD are considered key indicators for monitoring changes in climate extremes [61].

Table 2 presents the method to compute each index and its units. Nevertheless, an additional explanation is necessary for R95p. It is an index that indicates extreme daily precipitation and is obtained with a threshold corresponding to the precipitation value of the 95% percentile. Therefore, the percentile value can be used to measure the precipitation intensity, while the number of days in which the precipitation exceeds the percentile value indicates the frequency of the extreme events. The percentile is calculated for the historical and future periods to compare the precipitation intensity in these two periods. However, for comparing the frequency of the extreme events, we use as a threshold in both periods the 95% percentile computed to the historical period.

Table 2. Description of climate indices calculated in this study.

Variable	Short Name	Long Name	Index Definition	Unity
	PRCPTOT	Total precipitation	The accumulated seasonal precipitation over a given period. We are considering precipitation $Pr > 0$ instead of $Pr \geq 1 \text{ mm/day}$, as suggested by ETCCDI. The unit can be in mm or mm/day.	mm/day
	SDII	Simple precipitation intensity index	The ratio between the accumulated seasonal precipitation on wet days (days with $Pr \geq 1 \text{ mm/day}$) and the total number of wet days.	mm/day
P95 and R95p		95th percentile value and number of days with precipitation above the 95th percentile	Pr is the daily precipitation of a wet day ($Pr \geq 1 \text{ mm/day}$). Consider a certain period, for example, a sequence of summers. Initially, days with $Pr \geq 1 \text{ mm}$ are selected. Then, the 95th percentile is computed, and, subsequently, the number of days with Pr above the percentile value per summer can be identified. It gives the intensity (P95 value) and frequency (days in which $Pr > P95$) of the Pr extreme events. P95 is not a name defined by ETCCDI, but it is the threshold necessary for R95p.	mm/day and days
Daily Precipitation (Pr)	CDD	Consecutive dry days	The greatest number of consecutive days with $Pr < 1 \text{ mm/day}$. Consider, for instance, the summer of a given year, the longest sequence of dry days is then identified. The same is done for the other years. The final result can be presented on a map, in which the dry days' sequence is averaged for each grid point. Through this methodology, it is also possible to obtain the number of dry periods per time. This study considers a dry period if it is longer than five days. Unit: number of periods.	days
	CWD	Consecutive wet days	The greatest number of consecutive days with $Pr \geq 1 \text{ mm/day}$. Consider, for instance, the summer of a given year, the longest sequence of wet days is then identified. The same is done for the other years. The final result can be presented on a map, in which the wet days' sequence is averaged for each grid point. Through this methodology, it is also possible to obtain the number of wet periods per time period. This study considers a wet period if it is longer than five days. Unit: number of periods.	days

2.5. Analyses

The climate indices presented in Table 2 are computed by season for each member of the RCMs (Table 1) after their horizontal interpolation onto the CPC grid. However, for brevity, we focus on austral summer (December–January–February) since it is the wet period of the South American monsoon [22,24,43] and, therefore, a vast part of SA is susceptible to extreme events. The other seasons are presented in the online atlas.

Once we obtained the climate indices per single simulation, we computed the ensemble mean considering the three members of each RCM and the total ensemble (or multimodel ensemble) considering all models (nine simulations or members); Figure 2 is a flowchart exemplifying the methodology steps. Initially, we compare the performance of the ensembles in reproducing the climate indices during the historical period with that calculated using CPC. This validation is performed both subjectively and objectively; subjective because spatial patterns are visually compared between the models and the CPC, and objective since we calculated the spatial correlation between these data. The spatial correlations evaluation follows the criteria from Gilewski and Nawalani [62], according to which correlations equal to or less than 0.4 indicate poor model performance, corre-

lations between 0.4 and 0.6 suggest acceptable capability, correlations between 0.6 and 0.7 indicate satisfactory performance, values between 0.7 and 0.85 infer good skill, and correlations above 0.85 indicate a very good model achievement. Finally, the results are organized in maps that show the signal of the projected changes, i.e., the difference between each future period (2020–2039, 2040–2059, 2060–2079, and 2080–2099) and the historical period (1995–2014).

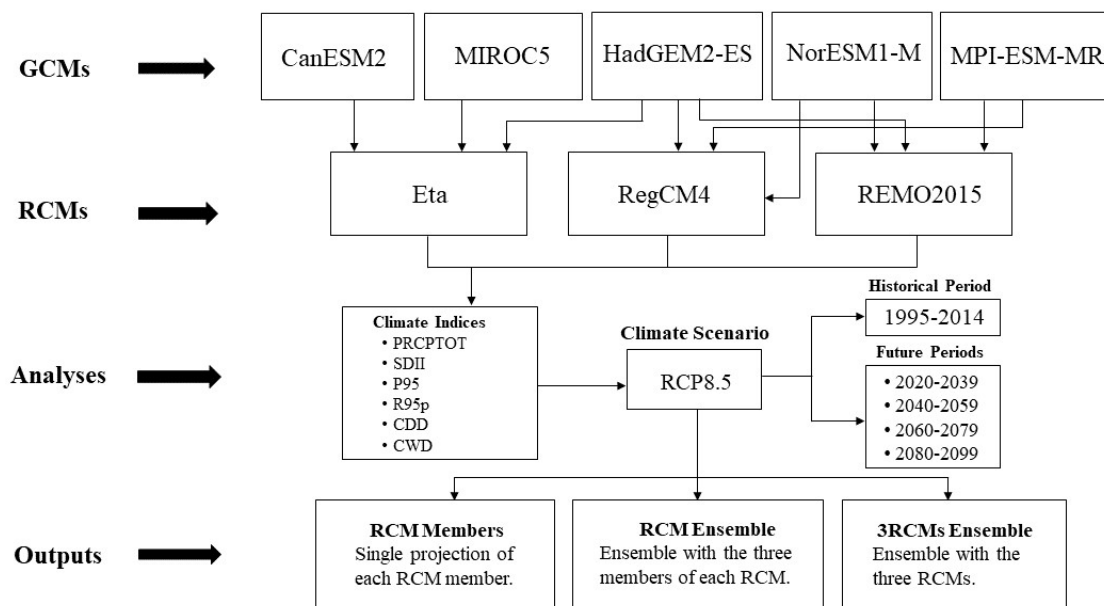


Figure 2. Flowchart describing the methodology steps.

For a more regional analysis of the projected changes over the two most important hydrological basins of South America (Amazon and La Plata), we calculated the seasonal average of the climate indices in subdomains shown in Figure 1, which are similar to Llopert et al. [25], being the Amazon limited by the coordinates 15° S–5° S and 68° W–52° W and the La Plata basin by 30° S–20° S and 60° W–50° W. The time series obtained for these subdomains are plotted to highlight the trends. Additionally, for the 3RCMs ensemble, the trends and their statistical significance ($\alpha = 0.05$) are calculated with the non-parametric test of Mann-Kendall (which can also be called the M-K test) [63–66]. A non-parametric test means that it can be applied to data with any statistical distribution. In the M-K test, the null hypothesis is that there is no monotonic trend in the series, while the alternate hypothesis is that a trend exists.

Concomitantly with this work, we developed an online atlas to provide the results of the climate indices for all seasons. The atlas is hosted in the domain of Universidade Federal de Itajubá and can be accessed at https://meteorologia.unifei.edu.br/south_america_climate_projection/CORDEX_ClimateIndices, accessed on 15 July 2022.

3. Results and Discussion

3.1. Present Climate

This section presents the performance of each RCM ensemble and the multimodel ensemble (3RCMs) in reproducing the main features of the SA precipitation during the austral summer (1995–2014) compared to the reference dataset (CPC). To highlight the spatial precipitation pattern in each ensemble, we show its mean value instead of the difference between the ensemble and the reference dataset, as in Kim et al. [38]. Moreover, the spatial correlation coefficient (r) calculated between each ensemble and CPC is also shown.

The precipitation climatology (or PRCPTOT) is characterized in CPC by a northwest-southeast band of higher volumes of precipitation extending from the Amazon to southeast Brazil (Figure 3a), which is the South Atlantic Convergence Zone (SACZ) [43,67]. In this

band, rainfall exceeds 6 mm/day. In other sectors of SA, there are lower volumes of precipitation. For instance, in southeastern SA, where the La Plata basin is located, it is higher than ~3 mm/day. The Eta ensemble performs better in simulating the SACZ than RegCM and REMO ensembles (Figure 3a–e). In addition, it is the ensemble with a better correlation with CPC ($r = 0.6$). RegCM underestimates the precipitation over southeastern Brazil, while REMO overestimates this variable over a large area in central SA, and their spatial correlation with CPC is 0.2 and 0.5, respectively. A common deficiency in all RCM ensembles is rainfall underestimation over northern SA. Over the Andes Mountains, there is rainfall overestimation, but it cannot totally be considered an error since there are also uncertainties in the reference dataset, and there are few stations in the Andes region to have their data assimilated by CPC analysis. Moreover, RCMs can reproduce the regional scale circulation improving the rainfall distribution in regions of complex topography. The visual analysis from Figure 3a–e indicates more similarity in precipitation volumes between 3RCMs and CPC. However, in terms of spatial correlation, it is slightly lower ($r = 0.5$) than Eta ($r = 0.6$), but in both, the correlation is considered acceptable (see Section 2.5). When the RCMs ensemble is compared with the GCMs ensemble from Reboita et al. [20] (https://meteorologia.unifei.edu.br/projecao_climatica/, accessed on 15 July 2022), it shows a large added value since PRCPTOT in the CGMs shows the maximum rainfall displaced from south Amazon to center-southeast Brazil, and a large area of rainfall over the Andes that is not observed in CPC (if the reader is interested only in the performance of GCMs over South America, see Díaz and Vera [68], Alves et al. [69], and Ortega et al. [70]). The deficiencies in PRCPTOT simulation by RCMs and GCMs may be due to the convective nature of the precipitation in austral summer, as suggested by Blázquez and Solman [47]. As rainfall is a parameterized variable, it is very dependent on the cumulus convection scheme used in the models.

In CPC, the precipitation intensity (SDII) during wet days ($Pr \geq 1 \text{ mm}$) shows higher intensity in the La Plata basin (Paraguay, Uruguay, and northeastern Argentina) and in spreading spots over the Amazonian region (Figure 3f). Over the La Plata basin, intense rainfall during summer is caused by the combination of the divergence associated with the subtropical upper-level jet, transport of warm and moist air from Amazon to southeastern SA by the Low-Level Jets eastern of the Andes (LLJs), and local convection [71], while in the Amazon the convection is the dominant mechanism. As a result, Eta (REMO) underestimated (overestimated) SDII in the La Plata basin and has better representation by RegCM. The main difference in the simulated SDII by the RCMs is the overestimation in the south and southeastern Brazil (Figure 3f–j). This feature also occurs in the 3RCMs ensemble. These differences justify the low spatial correlation between each ensemble and CPC, which are 0.5, 0.2, 0.5, and 0.4 in Eta, RegCM, REMO, and 3RCMs, respectively. These correlations are classified as unsatisfactory ($r \leq 0.4$) and acceptable ($0.4 < r < 0.6$) [62].

Moving to the indices that indicate extreme rainfall conditions, we start with P95 and R95p. The former is the 95th percentile of the daily precipitation and is used as a threshold to identify the days with extreme precipitation, i.e., R95p. P95 is also a way to compare the precipitation intensity or volume (since the unity is mm/day) among the RCMs ensemble. Figure 3k–o shows the spatial variability of P95. In CPC, the volume of daily precipitation is higher in the La Plata basin and western Amazon, as also shown in Solman and Blázquez [24] and Reboita et al. [20]. However, in the RCMs ensemble, higher daily precipitation is simulated over the south and southeast Brazil and the La Plata basin, which causes unsatisfactory and acceptable spatial correlations (varying from 0.3 in RegCM to 0.5 in REMO) in relation to CPC. RegCM and REMO simulate the area with higher P95 in the La Plata basin but with a large overestimation by REMO. While in this region, Eta underestimates P95, it is the ensemble with better performance in simulating P95 over the south and southeastern Brazil. All models have low performance over Amazon. These deficiencies are also reproduced in the 3RCMs ensemble (Figure 3o). CORDEX-phase 1 models also showed the same deficiencies [24]. In addition, the same problem occurs in GCMs [20,24].

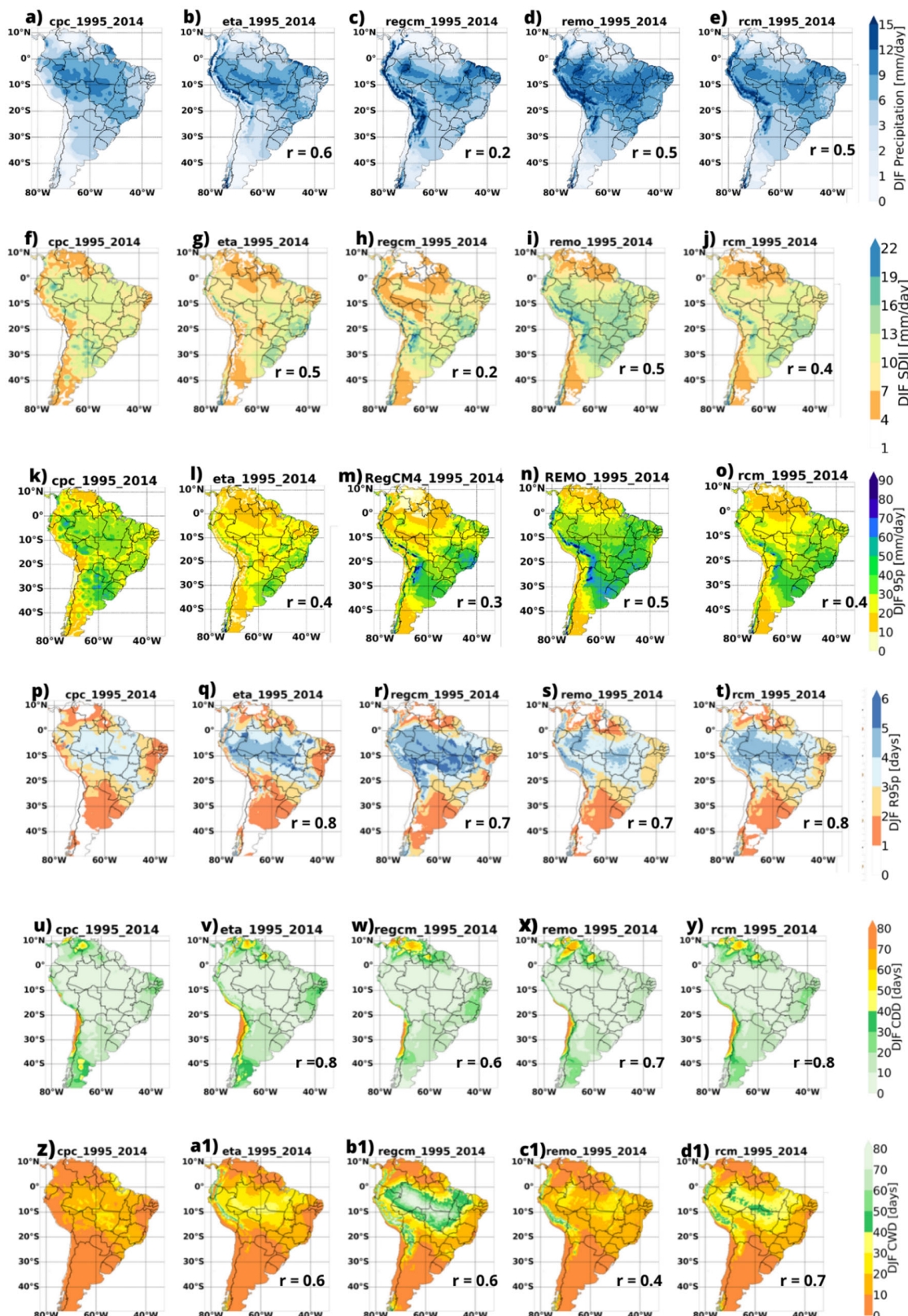


Figure 3. Climate indices calculated for the austral summer in the period of 1995–2014 using CPC (left column), each RCM ensemble (Eta, RegCM and REMO) and 3RCMs ensemble (right column): (a–e) PRCPTOT (mm/day), (f–j) SDII (mm/day), (k–o) P95 (mm/day), (p–t) R95p (days), (u–y) CDD (days), and (z,a1,b1,c1,d1) CWD (days). The values shown indicate the spatial correlation (r) between each ensemble and CPC.

While the La Plata basin has the most intense daily rainfall events, SACZ is the region with a higher frequency of extreme events (Figure 3p). It agrees with the different climatological characteristics of SA: SACZ is a persistent band of clouds and precipitation with a lifetime between 3 and 15 days [72–74]. On the other hand, in the La Plata basin, the precipitation is associated with mesoscale convective systems with a duration of no longer than 12 h [75–77]. In general, RCMs ensembles perform well in simulating R95p in the La Plata basin, but in the SACZ region, they overestimate it. Unlike the previous indices, R95p is well simulated by the REMO ensemble. Regarding spatial correlation, it is 0.7 in RegCM and REMO and 0.8 in Eta and 3RCMs in relation to CPC. When the RCMs ensemble is compared with the GCMs ensemble [20], the added value of RCMs becomes clear since GCMs show maxima of R95p over a large area from Peru to central Brazil.

Figures 3u–y and 3z,a1,b1,c1,d1 show CDD and CWD indices, respectively. CDD (CWD) corresponds to the average of the longest period of dry (wet) days each summer. RCMs ensemble represents well the spatial pattern and values of CDD, with spatial correlation coefficient ranging from satisfactory (0.6 in RegCM and 0.7 in REMO) to good (0.8 in Eta and 3RCMs). However, the RCMs' performance for CWD is slightly lower than CDD since they overestimate CWD in Amazon and neighborhoods. In terms of the correlation coefficient, it is 0.4 in REMO, 0.6 in Eta and RegCM, and 0.7 in 3RCMs. In most SA, long wet periods are a dominant feature in summer (Figure 3z,a1,b1,c1,d1), while CDD presents a shorter duration except in the extreme north and south of SA and over northeastern Brazil (Figure 3u–y). In this latter region, lasting CDD periods are also highlighted in the annual analysis of RCMs [17] and GCMs [78]. Longer dry periods are observed over the oceans in the region of the subtropical anticyclones (figure not shown), which are regions dominated by subsidence [79]. In CPC, the longest CWD occurs between south Amazon and central Brazil, not exceeding 40 days (Figure 3z,a1,b1,c1,d1), but this value is higher than 70 days in the RegCM ensemble, which is the model with a higher overestimate, and it affects the 3RCMs ensemble (Figure 3z,a1,b1,c1,d1). When the RCMs ensemble is compared with the GCMs ensemble in Reboita et al. [20], the spatial pattern and values of GCMs are closer to the RCMs for CDD, but large differences appear for CWD, which are the overestimates covering most of the continent.

The ensembles shown in Figure 3 indicate a good performance of RCMs in reproducing the SA climate. For this reason, they can be applied for studies of future climate. As discussed in Reboita et al. [20], differences in intensity of the simulated indices and that obtained with CPC are not a big issue because, in future climate studies, our interest is in the projected change signal obtained from the difference between future and historical periods.

3.2. Future Climate—Spatial Pattern of the Projected Changes

Future climate projections under the RCP8.5 scenario during austral summer are presented considering four time-slices (2020–2039, 2040–2059, 2060–2079, 2080–2099) since it allows us to visualize the time evolution of the projected changes.

The concern about climate change and its associated impact lies in water availability for human consumption, agriculture, and energy generation, for example. So, it is crucial to know the projected changes in seasonal rainfall amount. The changes projected in this variable (PRCPTOT) become stronger towards the end of the century in all RCMs ensembles (Figure 4). However, there are differences in the projected signals (uncertainties): while Eta projects a decrease in precipitation in the SACZ region and surroundings, RegCM and REMO project this same signal only over Amazon and wet conditions over center-southeast Brazil and La Plata basin. Although REMO has a more similar spatial pattern to RegCM, the intensity of the changes is weaker. Considering the projections of the 3RCMs ensemble (Figure 4d,h,l,p), they indicate drier conditions over Amazon and wetter conditions southward in this region, including the La Plata basin. Except for the Eta ensemble, the others are in line with the projections of CMIP6 models [80]. An interesting feature in Figure 4 is that the period 2040–2059 shows a weakening in the projected signal

compared to 2020–2039. The physical explanation is not clear, but it is a common feature in the projections across the different regions of the globe [81].

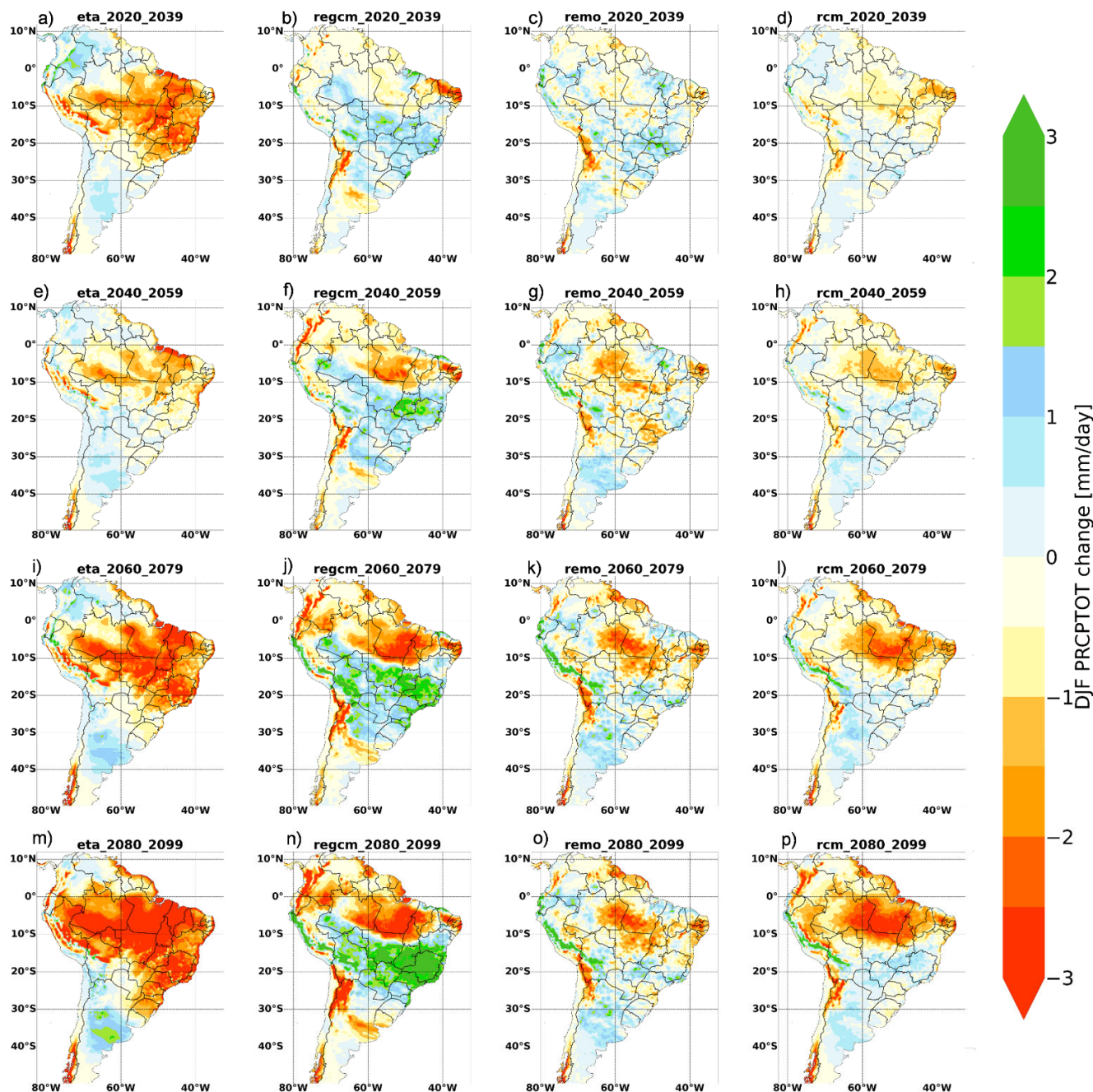


Figure 4. Changes projected to PRCPTOT (mm/day) during austral summer computed from each RCM ensemble (Eta, RegCM, and REMO) and 3RCMs ensemble (right column) and considering four time-slices: (a–d) 2020–2039, (e–h) 2040–2059, (i–l) 2060–2079, and (m–p) 2080–2099.

Uncertainties in climate projections can be associated basically with three factors: model (different numerical methods used to solve equations, physical parameterization schemes, and initial conditions, among other points), scenario (supposition of the future such as a world that injects more CO₂ into the atmosphere), and natural variability of the climate system [7,82–87]. In this study, we are using the same scenario (RCP8.5) but different RCMs. Besides, Eta is nested in two GCMs that are not used in RegCM and REMO. Therefore, these facts are the main source of uncertainties in this study. In AR5-IPCC, it

is acknowledged that there are uncertainties that we will never know and that the best response is to understand and cope with them [1].

Nevertheless, despite the uncertainties, the projection of increased PRCPTOT in the La Plata basin is in line with the trends documented using different datasets and periods of the present climate [88–90] and with other studies of future projections [19,25]. Projections of wetter conditions for southeastern Brazil seem to be an extension of the trends observed in the present climate [91]. For the present climate, Marengo et al. [91] and Céron et al. [90] have associated the increase of PRCPTOT with changes in the South Atlantic Subtropical Anticyclone (SASA) that acts as transporting moisture from the ocean to the southeastern SA. Moreover, it may also be the explanation in future scenarios. However, it is a subject that deserves more investigation since the location of anomalous high pressure in relation to the different sectors of SA can contribute to increasing or inhibiting precipitation in a specific location [92,93].

Another way to analyze the changes in rainfall is through SDII (Figure 5). The Eta ensemble (Figure 5a,e,i,m) projects a decrease in the precipitation intensity in most of Brazil and over the oceanic branch of SACZ (figure not shown) and an increase over northeast Argentina and Uruguay. On the other hand, RegCM and REMO project an increase of SDII between 10° and 40° S. The difference between these two models is that RegCM projects SDII decrease over northern Brazil while there are weak changes in REMO. In the 3RCMs ensemble (Figure 5d,h,l,p), the projected changes indicate SDII decrease over northern Brazil from the 2060–2079 period and an increase in this index over the La Plata basin from the 2020–2039 period.

While PRCPTOT provides a view of the seasonal accumulated precipitation, the extreme daily rainfall can be analyzed by P95 and R95p indices. Episodes of extreme daily rainfall are not an exclusive characteristic of the future years since they have been more frequent and intense in the present climate [21,94] and are often responsible for floods and landslides. The World Meteorological Organization (WMO) [95] published the “State of Climate in 2021”, describing many extreme precipitation events and their impacts across the globe. Moreover, extremely devastating were the two episodes of intense rainfall in Petrópolis city in southeastern Brazil in 2022. The first episode occurred on 15 February, in which a rainfall of 260 mm in only one day caused floods and landslides [96,97]. After one month, on 20 March, another extreme precipitation event struck Petrópolis with daily total precipitation of 534.4 mm [97,98]. Here, the declaration by Fisher et al. [99] is very opportune: “These record-shattering extremes, nearly impossible in the absence of warming, are likely to occur in the coming decades”. Both events in Petrópolis were responsible for more than 230 deaths [100]. Our study indicates that the intensity (Figure 6) and the frequency (Figure 7) of the daily precipitation events are projected to increase with time in most SA. However, extreme values such as those registered in Petrópolis do not appear in Figure 6 since they are in the tail of the statistical data distribution.

Figure 6 shows the climate change signal of the daily precipitation percentile of 95% (a measure of rainfall intensity) of 2015–2099 in relation to the 1995–2014 period. Even Eta model projects an increase in P95 over south/southeast Brazil and the La Plata basin (Figure 6a–d). RegCM and REMO also show an increase over central Brazil, which influences the 3RCMs ensemble (Figure 6m). Between northeastern Argentina and Uruguay, P95 overtakes 50 mm/day in REMO individual members and ensemble (Figure 6i–l).

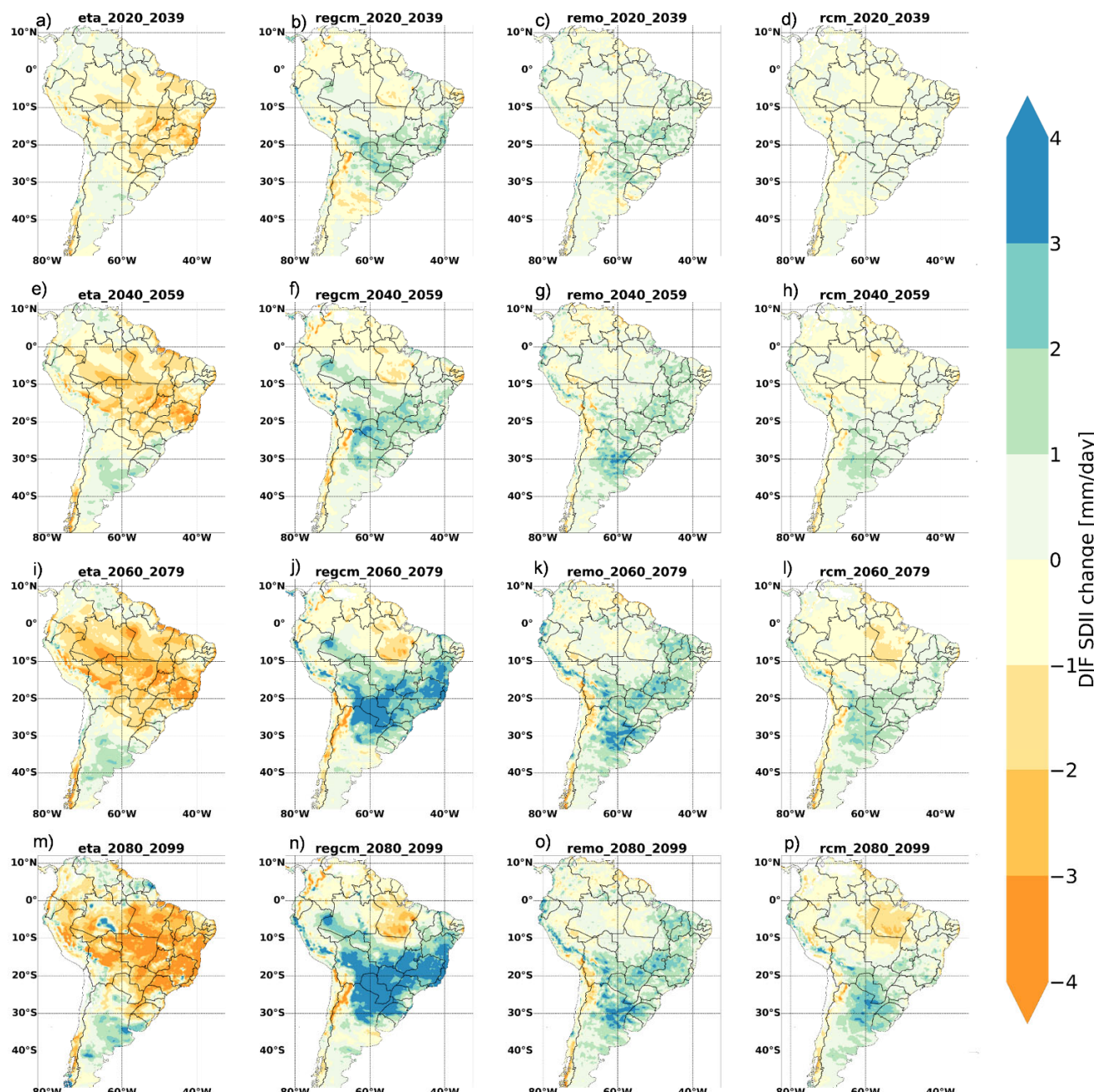


Figure 5. Changes projected to SDII (mm/day) during austral summer computed from each RCM ensemble (Eta, RegCM, and REMO) and 3RCMs ensemble (right column) and considering four time-slices: (a–d) 2020–2039, (e–h) 2040–2059, (i–l) 2060–2079, and (m–p) 2080–2099.

While Figure 6 shows a higher increase of P95 over the La Plata basin in all RCMs, regions with a higher frequency of extreme events differ in each RCM ensemble (Figure 7). The frequency of the extreme events in all time-slices is computed based on the threshold obtained for the historical period, i.e., P95 of the 1995–2014 period.

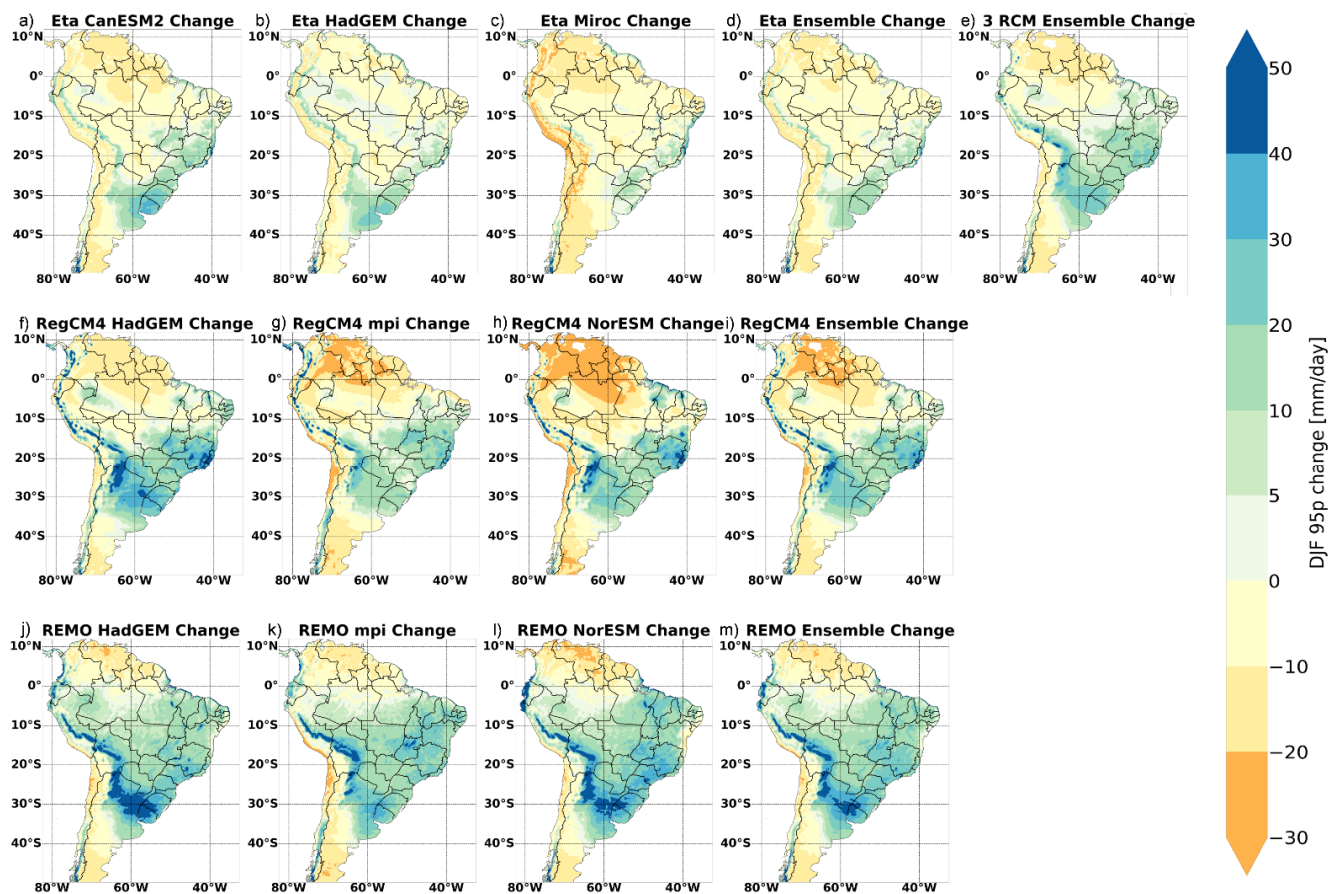


Figure 6. Changes projected to P95 (mm/day) during austral summer computed from each member of: (a–d) Eta, (f–i) RegCM, and (j–m) REMO individual ensembles, and (e) 3RCMs ensemble. Changes in the percentile of 95% are obtained with the difference obtained in the 2015–2099 and 1995–2014 periods.

The Eta ensemble projects a higher frequency of rainfall precipitation extremes (~2–3 events per summer) over Argentina and a decrease over most of SA (Figure 7a,e,i,m). RegCM projects an increase over the SACZ region and a decrease over northern Brazil (Figure 7b,f,j,n), whilst REMO has a spatial pattern similar to RegCM but with a weaker signal (Figure 7c,g,k,o). The contrasting signal changes between Eta and the other RCMs (uncertainties) cause a weak signal in the 3RCMs ensemble, which projects a decrease in extreme rainfall frequency over northern Brazil (~3 events) and an increase (~1–2 events) in most of the continent in all time-slices (Figure 7d,h,e,p).

Physically explaining how climate change influences individual weather or climate extreme events is not simple [101]. There are different natural (e.g., natural variability of the climate: teleconnection patterns) and anthropogenic factors (e.g., greenhouse gases increase, aerosol effects etc.) combined to produce the specific conditions of an event. For this reason, a new area in meteorology called event attribution measures how ongoing climate change directly affects recent extreme weather events [101,102].

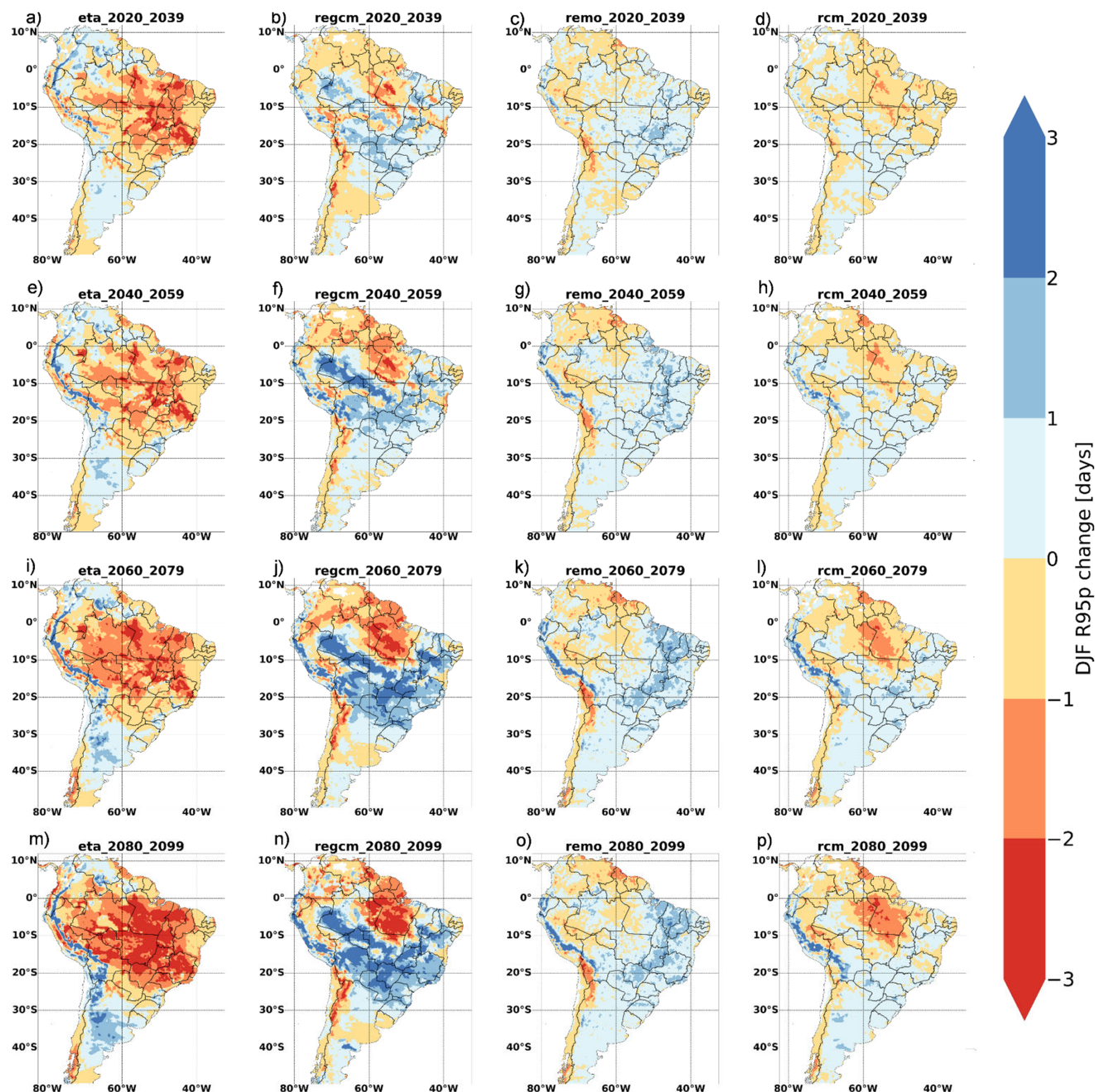


Figure 7. Changes projected to R95p (days) during austral summer computed from each RCM ensemble (Eta, RegCM, and REMO) and 3RCMs ensemble (right column) and considering four time-slices: (a–d) 2020–2039, (e–h) 2040–2059, (i–l) 2060–2079, and (m–p) 2080–2099. R95p in all time-slices is obtained with the same threshold (P95) calculated for the 1995–2014 period.

Here, a general view of the influence of climate change on extreme events is provided. The climate system is becoming more complex as more energy is added to this system, which is not at the same rate in all regions of the planet. The atmosphere manifests itself in climate system warming, developing stronger weather systems to get a homogenous spatial distribution of temperature (for example, extratropical cyclones transport warm and moist air toward the poles); a consequence of this process is heavier rainfall. Nevertheless, we also need to consider the impact of the warming on large-scale atmospheric circulation and its remote response to local weather. In this thinking line, global warming may modify the teleconnection patterns' location/intensity/frequency (such as El-Niño and La Niña, Indian

Ocean Dipole, etc.). Consequently, these patterns affect the local weather systems across the globe, which may respond through extreme rainfall events. However, even the changes in temperature and precipitation on a local scale can affect atmospheric stability leading to strong convective thunderstorms and intense rainfall [33]. From thermodynamics, warm air can hold more water vapor in the atmosphere, and as it is a greenhouse gas, there is positive feedback for planet warming [103]. According to the Clausius-Clapeyron equation, the water-holding capacity of the atmosphere has been estimated to increase by ~7% per K [104]. Adding extra water to the atmosphere and the changes in atmospheric circulation can lead to extreme events of precipitation (e.g., Pfahl et al. [105]). However, the increase in the water vapor in the atmosphere is not documented at the same rate across the globe since there are several local factors affecting the atmosphere and the influence of different atmospheric circulation patterns in distinct regions—one example can be seen in Chai et al. [106] for Asia. Since the pre-industrial era, the global average temperature has risen by 1.1 °C [47,107]. The approximately linear observed global warming trend of ~0.2 °C/decade has been evidenced since about 1980, but a nonlinear increase in the number of extreme heat events has also been observed [108]. Recently, in May 2022, parts of Pakistan and northwest India registered extreme temperatures reaching more than 50 °C [109], and in July 2022, severe heat reached Europe, causing more than 40 °C in parts of the United Kingdom [110]. These extreme temperatures affect evaporation, but the places with higher evaporation may not receive water through precipitation since the winds advect the air masses far from their source. Consequently, dry conditions can develop in such regions.

Concerning SA, projections of intense precipitation do not occur over the whole continent. However, a weakening in the rainfall intensity is projected over northern SA and may be related to the changes in the speed of trade winds in future scenarios and the weak surface-atmosphere coupling [22]. Trade winds are projected to weaken [9,19,111], decreasing the moisture flux convergence over part of Amazon and north of SA [32]. Another factor that may contribute to reduced rainfall is that within an atmosphere with higher CO₂ concentration, there is an influence of the physiological response of vegetation on climate, as stomatal closure has been observed [112], leading to lower total evaporation and reduced water loss during photosynthesis [113,114].

On the other hand, the projected changes in atmospheric circulation by RegCM have shown an anticyclonic pattern over the southwestern Atlantic Ocean (figure not shown), contributing to moisture transport from this ocean to subtropical latitudes of SA, which includes the La Plata basin [111]. This anomalous anticyclonic pattern may result from the projected decrease in cyclones frequency over the South Atlantic Ocean [30,111]. One evidence of the high-pressure anomalies in the projections is the sea surface warming in the same region with pressure anomalies [115], which means that in a high pressure area, there is a decrease in cloudiness, allowing the energy to warm the surface. Precipitation in the La Plata basin also has a contribution of surface-atmosphere interaction, which is projected to strengthen during the austral summer [22]. Therefore, the availability of moisture over the La Plata basin as well as over southern Brazil associated with the surface warming drives a robust increase in the Convective Available Potential Energy (CAPE) that, associated with an increase in the vertical wind shear, produces the ideal conditions for severe weather in the mentioned places mainly in RCP8.5 scenario [33].

In order to complement the extreme precipitation events discussion, it is essential to know if the projections of wet and dry consecutive days indicate lasting or shorter periods (number of days). A general view of Figures 8 and 9 shows that regions with a shorter (lasting) period of CWD are characterized by lasting (shorter) CDD. In the case of CWD (Figure 8), RCM ensembles project a consistent and more prominent change of shorter periods of CWD over Amazon. This signal is more intense in the RegCM ensemble and at the end of the century, when a decrease of more than 30 days may occur in the wet spells (Figure 8b,f,j,n). The lasting dry spells are projected over the extreme north of SA, which is a consistent signal among the RCM ensembles. A possible explanation is the weakening moisture flux convergence projected over this region in climate scenarios [32].

The Eta ensemble also projects more lasting periods of CDD over northeastern Brazil (Figure 9a,e,i,m). As it is the second driest region in South America—known as Brazilian semi-arid—projections of increasing CDD should cause more negative impacts on life in this region [20]. Lasting CDD over the extreme north of SA and Brazilian semi-arid also has a more intense signal in the annual analysis, as shown by Almazroui et al. [80].

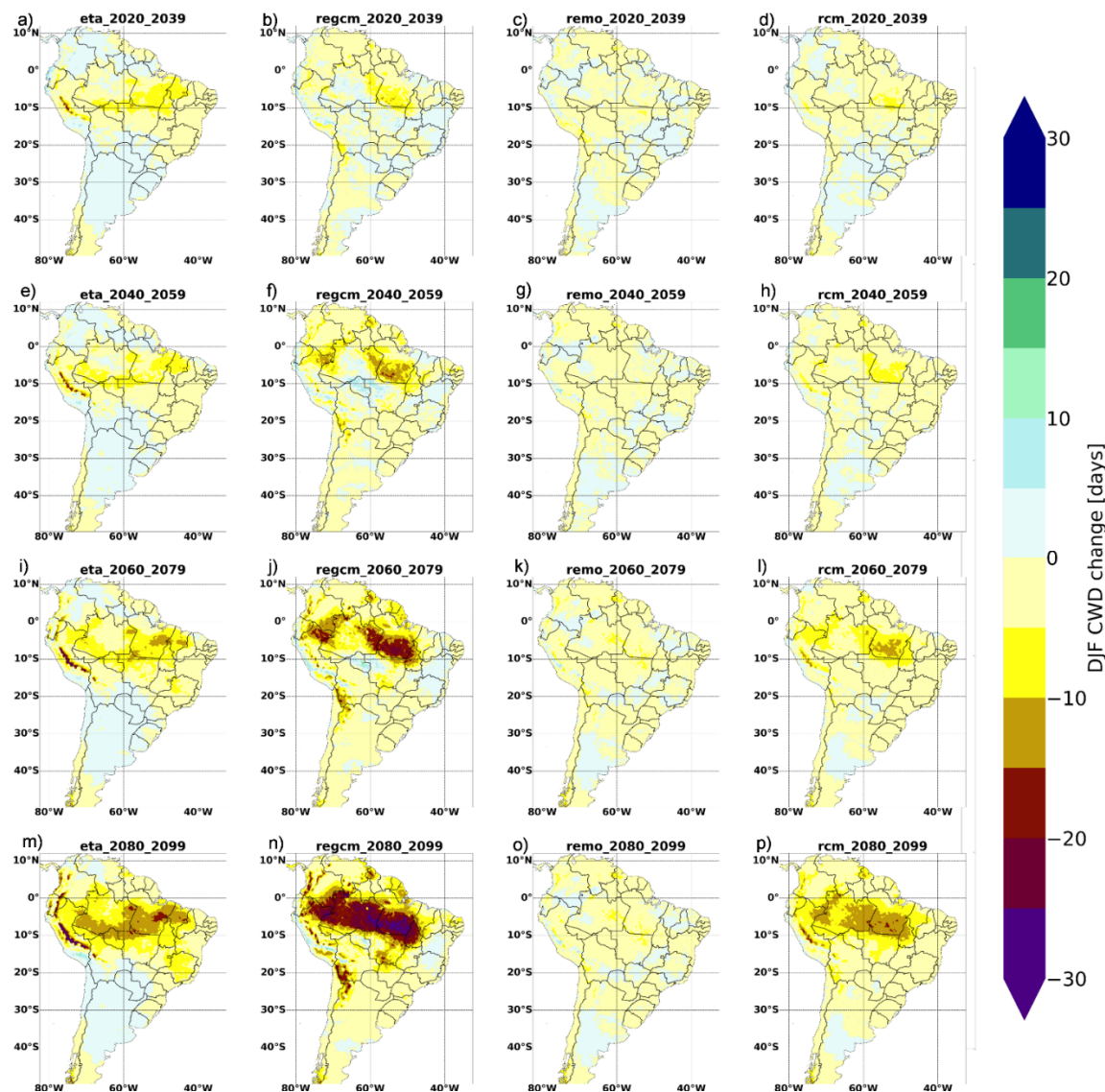


Figure 8. Changes projected to CWD (days) during austral summer computed from each RCM ensemble (Eta, RegCM, and REMO) and 3RCMs ensemble (right column) and considering four time-slices: (a–d) 2020–2039, (e–h) 2040–2059, (i–l) 2060–2079, and (m–p) 2080–2099.

Although weak, the signal of increasing CWD covers a larger area of the southeastern SA in Eta than in the other RCM ensembles (Figure 8). The same pattern is projected by the Eta ensemble for the decrease in CDD, while RegCM and REMO show a decrease over parts of southeastern Brazil (Figure 9). We also computed the number of periods longer than five days with dry and wet spells (figures not shown). All RCM ensembles consistently show a decrease of ~2 CWD periods in northern SA, but the Eta ensemble also projects a decrease over north and northeast Brazil. In terms of increasing the number of CWD periods, it is projected over the La Plata basin by Eta and the SACZ by RegCM, while REMO projects almost no changes. In general, regions with decreasing (increasing) CWD

periods are characterized by increasing (decreasing) CDD, but the changes do not overtake the two periods even at the end of the century (2080–2099).

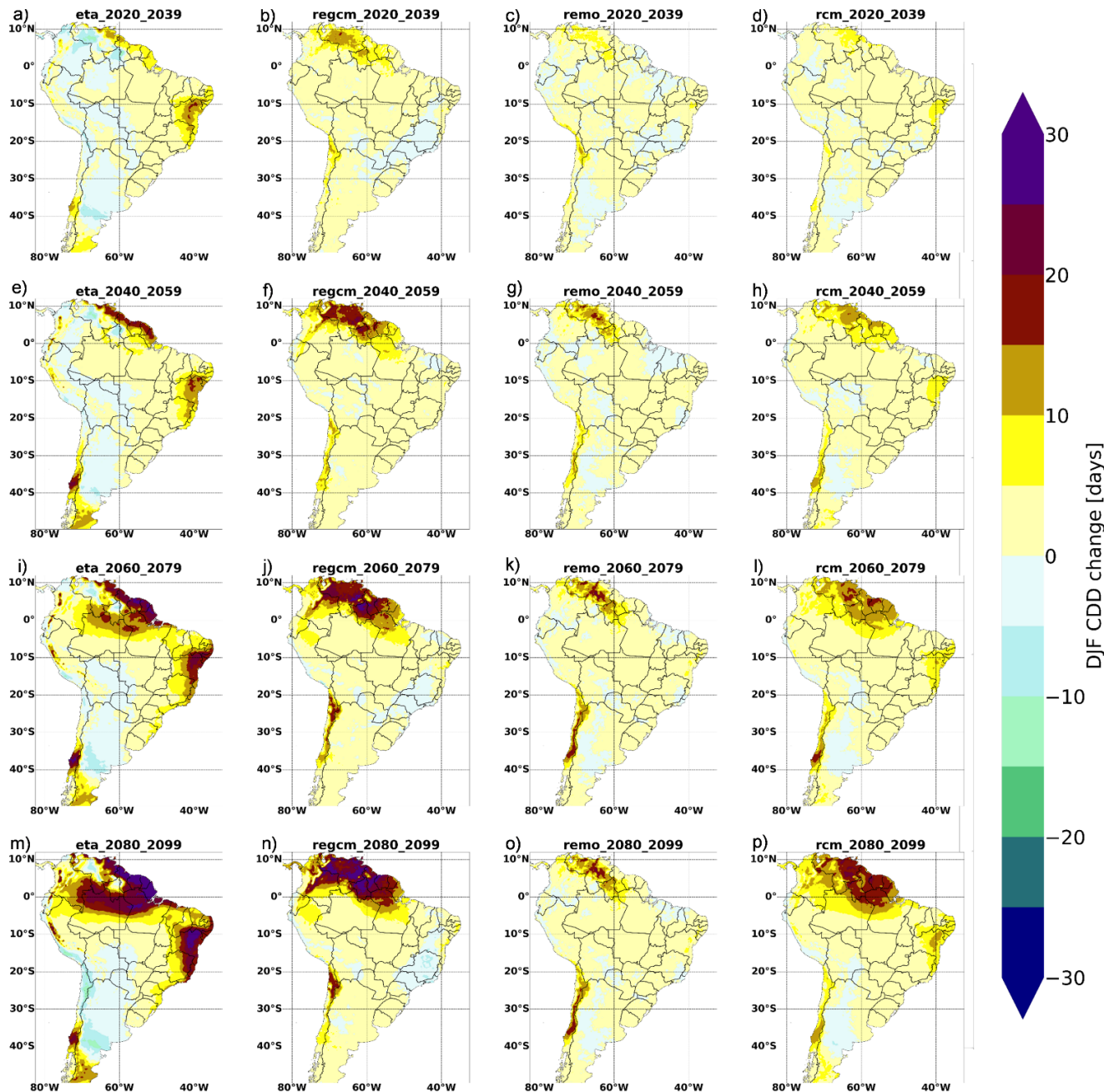


Figure 9. Changes projected to CDD (days) during austral summer computed from each RCM ensemble (Eta, RegCM, and REMO) and 3RCMs ensemble (right column) and considering four timeslices: (a–d) 2020–2039, (e–h) 2040–2059, (i–l) 2060–2079, and (m–p) 2080–2099.

3.3. Trends

This section presents the trends and their statistical significance test calculated for the climate indices projected by the 3RCMs ensemble during the austral summer (Table 3). In order to compare our results (Eta, RegCM, and REMO with grid space of 25 km) with the multimodel ensemble (RCA, REMO, and RegCM with grid space of 50 km) performed by Llopert et al. [25], we used two subdomains (AMZ and LPB in Figure 1) similar to those authors and computed areal means of the climate indices.

Table 3. Trend slopes (per year) obtained for the AMZ and LPB time series. All values presented statistically significant trends ($\alpha = 0.05$), except PRCPTOT for LPB.

Index	Slopes for AMZ	Slopes for LPB
PRCPTOT (mm/day)	-0.0124	0.0040
SDII (mm/day)	-0.0075	0.0168
R95p (days)	-0.0059	0.0052
CWD (days)	-0.0873	-0.0092
CWD periods > 5 days	-0.0024	-0.0016
CDD (days)	0.0185	0.0099
CDD periods > 5 days	0.0013	0.0022

The methodology is exemplified in Figure 10 for SDII in LPB. After calculating the areal mean of the summer projections in each RCM member, we computed the ensemble mean of the 3RCMs. In the sequence, the difference between each summer and the historical average is calculated (it provides the signal of the climate change), which is the information shown in Figure 10. This kind of figure (also known as spaghetti) allows us to see the spreading between the members of the ensemble and, consequently, the uncertainties. In the case of SDII in LPB, Eta_CanESM2 (continuous red line) shows a negative trend, while the members of RegCM and REMO (blue and green lines) show a positive trend. A positive trend is a dominant signal in the 3RCMs ensemble (bold black line). For the 3RCMs ensemble, the trend and its statistical significance are computed (Table 3). We applied this methodology to all the climate indices, and the results are summarized in Table 3. Note that the trend value is per summer, which means that if we need to know it per decade, we need to multiply the trend value by ten. Besides, if the index unity is in mm/day, we must multiply by 90. Another information is that the positive slope indicates a positive trend and the opposite for a negative value.

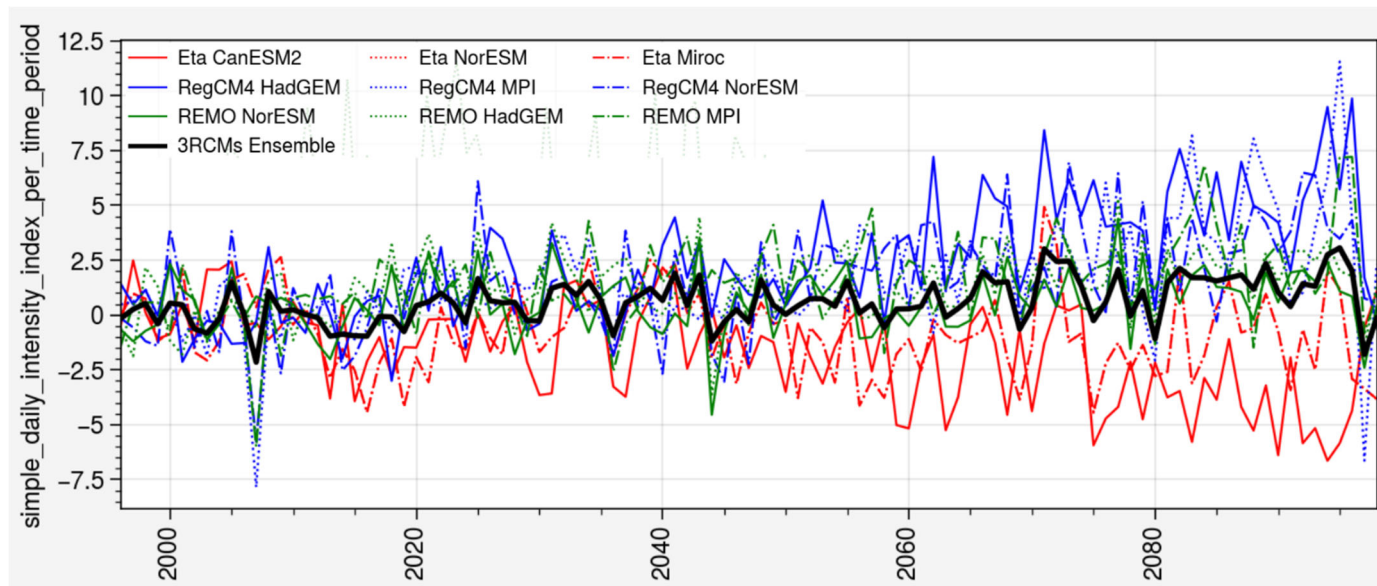


Figure 10. SDII trend time series (1995–2099) of all RCMs members and the 3RCMs ensemble (continuous black line), considering the historical average of 1995–2014 during austral summer in the LPB.

In a general view of Table 3 for AMZ, all indices related to increase in volume (PRCPTOT), intensity (SDII), and frequency (R95p and CWD) of rainfall show negative trends while the dry spells (CDD) present positive trends. In other words, dry conditions are projected for the AMZ subdomain towards the end of the century. On the other hand, in the LPB subdomain, 3RCMs ensemble project increase in the volume (PRCPTOT) and intensity

(SDII) of rainfall and in the frequency of extreme events (R95p); but there is a negative trend in the duration of the consecutive wet days and positive trend for consecutive dry days. It indicates that the precipitation may occur more concentrated in short periods, which causes extreme events and damage to society.

The projected changes for PRCPTOT in the subdomain AMZ show a negative and significant trend, while in LPB, it is positive and not significant (Table 3). In Figure 1, note that the LPB subdomain is located more over the dry part of the basin (see Figure 3), and it causes the absence of a significant trend. Comparing these results with Llopert et al. [25], while our PRCPTOT shows a negative and significant trend, Llopert et al. [25] obtained positive values of changes but without a trend in the RCM ensemble. Here, the dry conditions are more impacted by the Eta model, which is not included in the ensemble of those authors. For the LPB subdomain, both studies indicate positive trends, but here without statistical significance. The positive trend in LPB is a common signal in studies using GCMs/RCMs and climate scenarios [19,25,80].

4. Conclusions

A multimodel ensemble was performed with three RCMs (Eta, RegCM, and REMO) under the CORDEX-CORE framework for South America to show changes projected in the precipitation described by six climate indices based on the ETCCDI methodology. The indices were evaluated under RCP8.5 regarding their spatial variability and time evolution (time-slices: 2020–2039, 2040–2059, 2060–2079, and 2080–2099). As previous studies showed that RCMs added value compared to their driven GCMs, we focused only on RCMs and in the wettest period of most of South America (December–January–February). In addition, special attention was given to Amazon and La Plata basins, the most important watershed on the continent.

The ensemble construction was performed for each RCM and, after, for the three RCMs (called 3RCMs ensemble). Regarding climate projections, the Eta ensemble generally shows differences in the projected signals compared with RegCM and REMO ensembles, mainly in the SACZ region, where Eta projects dry conditions and the other ensembles wet conditions (a prominent region of uncertainty). On the other hand, the ensembles are consistent in the dry conditions over northern South America and the wet conditions in the La Plata basin, and this consistency also occurs in terms of the different climate indices. The projected signals by the 3RCMs ensemble generally follow those from RegCM and REMO and are more intense at the end of the century.

In order to summarize the results and answer the scientific questions presented in Section 1, a schematic figure was elaborated (Figure 11) considering the time-slice representative of the end of the century obtained by the 3RCMs ensemble.

The most consistent signal of change is located where more than one climate index indicates changes, and it occurs over a large area of Amazon and north of South America, and the La Plata basin:

- Extreme north of South America: the decrease in PRCPTOT is accomplished by an increase in CDD periods;
- Western Amazon: the decrease in PRCPTOT is accomplished by a decrease in CWD periods;
- Eastern Amazon (north Brazil): the decrease in PRCPTOT is accomplished by a decrease in SDII, CWD, and R95p;
- Semi-arid Brazil (northeast of South America): it is located in a transition region in PRCPTOT and is dominated by an increase in CDD; the southern of this area also shows an increase of R95p;
- La Plata basin (a region that coincides with the dashed line in Figure 11): the increase in PRCPTOT, SDII, and R95p coincides with a decrease in CDD;
- Southern Argentina: the increase in PRCPTOT and R95p occurs concomitantly with a decrease in CDD.

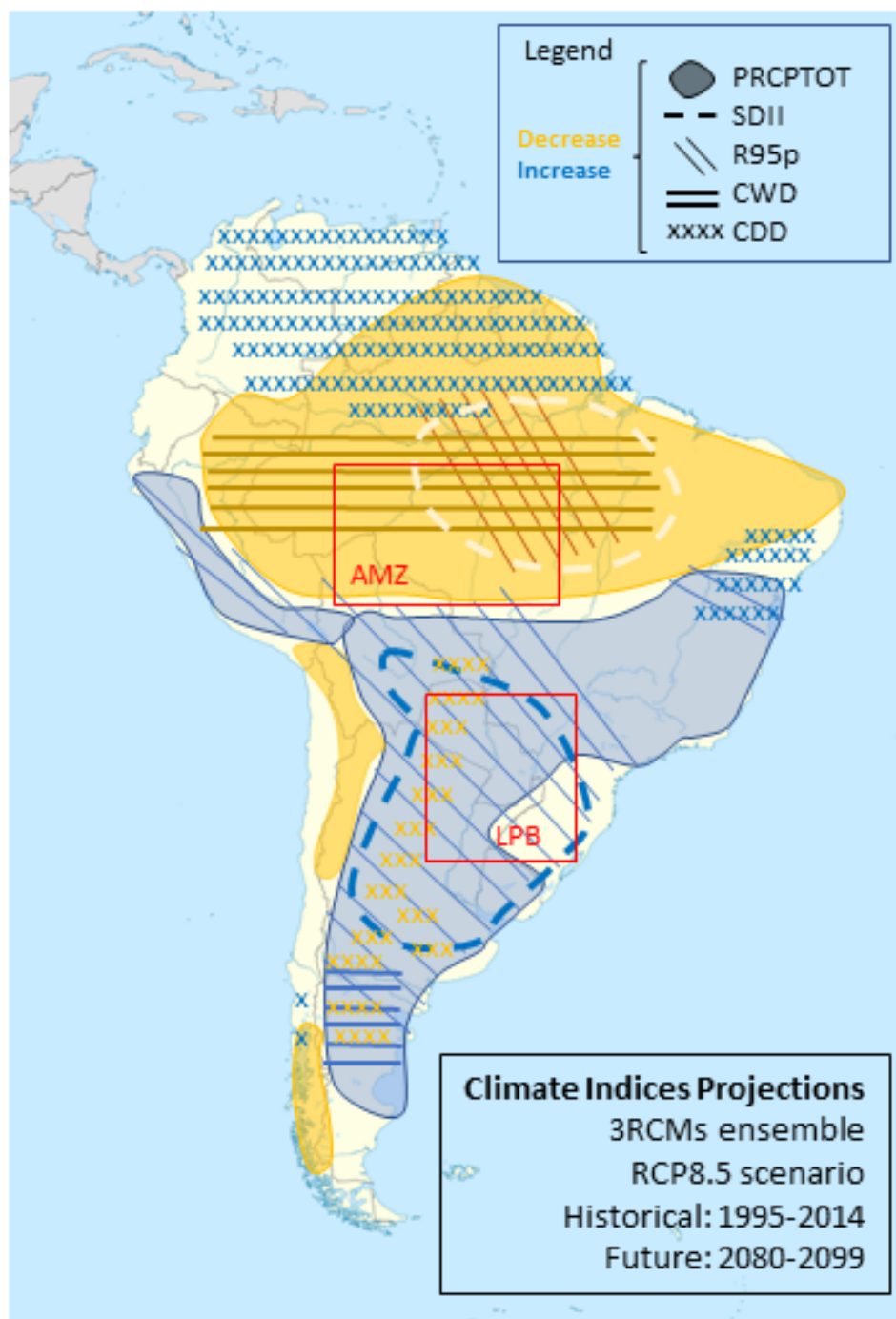


Figure 11. Schematic representation of the projected changes for the precipitation climate indices based on the 3RCMs ensemble under RCP8.5 at the end of the century (2080–2099). Red boxes indicate the location of the subdomains in the Amazon and La Plata basins.

This study highlights the increase in dry and wet extreme events over South America in future decades under global warming. However, it also emphasizes that different RCMs respond to climate change differently, representing a crucial uncertainty in climate change research (such as in southeastern Brazil).

As extreme climate (CDD, CWD) and weather (R95p) events affect the distribution of the species, human health, freshwater availability, agriculture, fires, and energy supply, such events need to be considered when designing critical infrastructures, such as power plants and homes. In addition, R95p is a major source of floodings and landslides in

vulnerable areas. Therefore, this work is essential for stakeholders to implement adaptation and mitigation strategies to avoid human and economic losses. Notwithstanding, we underline that a complex environment of factors, including appropriate metrics for risk analysis, the regular evaluation and review of analysis methods, and the need to implement mitigating measures at global, continental, regional, and local levels, hinder decision-making potentiality. In this scenario, not only research on the effects of climate change is urgent but also advances that contribute to stakeholder engagement on climate adaptation and better risk management, such as alert systems focused on impacts, inter-municipal organizations, partnerships between stakeholders, and closer dialogue between academia and stakeholders.

Author Contributions: Conceptualization, M.S.R.; methodology, M.S.R. and R.P.d.R.; software, C.A.d.S., T.C.B. and P.L.L.d.S.S.; formal analysis, T.C.B., P.L.L.d.S.S., G.W.S.F. and M.S.R.; writing—original draft preparation, G.W.S.F., M.S.R. and R.P.d.R.; writing—review and editing, G.W.S.F. and M.S.R. All authors have read and agreed to the published version of the manuscript.

Funding: The authors gratefully acknowledge the financial support from Coordination for the Improvement of Higher Education Personnel (CAPES, Finance Code 001), CNPq, FAPEMIG, ENGIE, ENERGISA, MC&E, and the R&D project from the Brazilian National Electric Energy Agency (ANEEL).

Institutional Review Board Statement: Not applicable.

Informed Consent Statement: Not applicable.

Data Availability Statement: All datasets used in this study are available on public online databases.

Acknowledgments: The authors acknowledge all meteorological centers that provided the data/models used in this study.

Conflicts of Interest: The authors declare no conflict of interest. The funders had no role in the design of the study; in the collection, analyses, or interpretation of the data; in the writing of the manuscript; or in the decision to publish the results.

References

- IPCC. Climate change 2014: Synthesis report. In *Contribution of Working Groups I, II and III to the Fifth Assessment Report of the Intergovernmental Panel on Climate Change*; Pachauri, R.K., Meyer, L.A., Eds.; IPCC: Geneva, Switzerland, 2014; Available online: <https://www.ipcc.ch/report/ar5/syr/> (accessed on 15 July 2022).
- IPCC. Climate change 2021: The physical science basis. In *Contribution of Working Group I to the Sixth Assessment Report of the Intergovernmental Panel on Climate Change*; Masson-Delmotte, V., Zhai, P., Pirani, A., Connors, S.L., Péan, C., Chen, Y., Goldfarb, L., Gomis, M.I., Matthews, J.B.R., Berger, S., et al., Eds.; Cambridge University Press: Cambridge, UK, 2021; Available online: <https://www.ipcc.ch/report/ar6/wg1/#FullReport> (accessed on 15 July 2022).
- Zilli, M.T.; Carvalho, L.M.V.; Liebmann, B.; Silva Dias, M.A. A comprehensive analysis of trends in extreme precipitation over southeastern coast of Brazil. *Int. J. Climatol.* **2017**, *37*, 2269–2279. [[CrossRef](#)]
- Ruddiman, W.F. *Earth's Climate: Past and Future*; W.H. Freeman & Company: New York, NY, USA, 2008.
- Trenberth, K. More knowledge, less certainty. *Nat. Rep. Clim. Chang.* **2010**, *1*, 20–21. [[CrossRef](#)]
- Nearing, G.S.; Tian, Y.; Gupta, H.V.; Clark, M.P.; Harrison, K.W.; Weijs, S.V. A philosophical basis for hydrological uncertainty. *Hydrol. Sci. J.* **2016**, *61*, 1666–1678. [[CrossRef](#)]
- Kundzewicz, Z.W.; Krysanova, V.; Benestad, R.E.; Hov, Ø.; Piniewski, M.; Otto, I.M. Uncertainty in climate change impacts on water resources. *Environ. Sci. Policy* **2018**, *79*, 1–8. [[CrossRef](#)]
- Folke, C.; Polasky, S.; Rockström, J.; Galaz, V.; Westley, F.; Lamont, M.; Scheffer, M.; Österblom, H.; Carpenter, S.R.; Chapin, F.S.; et al. Our future in the Anthropocene biosphere. *Ambio* **2021**, *50*, 834–869. [[CrossRef](#)]
- Ambrizzi, T.; Reboita, M.S.; da Rocha, R.P.; Llopert, M. The state of the art and fundamental aspects of regional climate modeling in South America. *Ann. N. Y. Acad. Sci.* **2019**, *1436*, 98–120. [[CrossRef](#)]
- Eyring, V.; Bony, S.; Meehl, G.A.; Senior, C.A.; Stevens, B.; Stouffer, R.J.; Taylor, K.E. Overview of the Coupled Model Intercomparison Project Phase 6 (CMIP6) experimental design and organization. *Geosci. Mod. Dev.* **2016**, *9*, 1937–1958. [[CrossRef](#)]
- Giorgi, F.; Jones, C.; Asrar, G. Addressing climate information needs at the regional level: The CORDEX framework. *WMO Bull.* **2009**, *58*, 175–183. Available online: <https://public.wmo.int/en/bulletin/addressing-climate-information-needs-regional-level-cordex-framework> (accessed on 1 July 2022).
- CORDEX CORE Simulations—CORDEX Coordinated Output for Regional Evaluations (CORE). Available online: <https://cordex.org/experiment-guidelines/cordex-core/cordex-core-simulations/> (accessed on 8 August 2022).

13. Giorgi, F. Introduction to the special issue: The phase I CORDEX RegCM4 hyper-matrix (CREMA) experiment. *Clim. Chang.* **2014**, *125*, 1–5. [[CrossRef](#)]
14. Giorgi, F.; Coppola, E.; Teichmann, C.; Jacob, D. Editorial for the CORDEX-CORE experiment I special issue. *Clim. Dyn.* **2021**, *57*, 1265–1268. [[CrossRef](#)]
15. Giorgi, F.; Coppola, E.; Solmon, F.; Mariotti, L.; Sylla, M.B.; Bi, X.; Branković, C. RegCM4: Model description and preliminary tests over multiple CORDEX domains. *Clim. Res.* **2012**, *52*, 7–29. [[CrossRef](#)]
16. Remedio, A.R.; Teichmann, C.; Buntемeyer, L.; Sieck, K.; Weber, T.; Rechid, D.; Hoffmann, P.; Nam, C.; Kotova, L.; Jacob, D. Evaluation of new CORDEX simulations using an updated Köeppen–Trewartha climate classification. *Atmosphere* **2019**, *10*, 726. [[CrossRef](#)]
17. Chou, S.C.; Lyra, A.; Mourão, C.; Dereczynski, C.; Pilotto, I.; Gomes, J.; Chagas, D. Evaluation of the Eta simulations nested in three global climate models. *Am. J. Clim. Chang.* **2014**, *3*, 438. [[CrossRef](#)]
18. Giorgi, F.; Coppola, E.; Raffaele, F.; Diro, G.T.; Fuentes-Franco, R.; Giuliani, G.; Mamgain, A.; Llopard, M.; Mariotti, L.; Torma, C. Changes in extremes and hydroclimatic regimes in the CREMA ensemble projections. *Clim. Chang.* **2014**, *125*, 39–51. [[CrossRef](#)]
19. Reboita, M.S.; da Rocha, R.P.; Dias, C.G.; Ynoue, R.Y. Climate projections for South America: RegCM3 driven by HadCM3 and ECHAM5. *Adv. Meteorol.* **2014**, *2014*, 376738. [[CrossRef](#)]
20. Reboita, M.S.; Kuki, C.A.C.; Marrafon, V.H.; de Souza, C.A.; Ferreira, G.W.S.; Teodoro, T.A.; Lima, J.W.M. South America climate change revealed through climate indices projected by GCMs and Eta-RCM ensembles. *Clim. Dyn.* **2022**, *58*, 459–485. [[CrossRef](#)]
21. Dereczynski, C.; Chou, S.C.; Lyra, A.; Sondermann, M.; Regoto, P.; Tavares, P.; Skansi, M.M. Downscaling of climate extremes over South America—Part I: Model evaluation in the reference climate. *Weather Clim. Extrem.* **2020**, *29*, 100273. [[CrossRef](#)]
22. Teodoro, T.A.; Reboita, M.S.; Llopard, M.; da Rocha, R.P.; Ashfaq, M. Climate change impacts on the South American monsoon system and its surface–atmosphere processes through RegCM4 CORDEX-CORE projections. *Earth Syst. Environ.* **2021**, *5*, 825–847. [[CrossRef](#)]
23. Falco, M.; Carril, A.F.; Menéndez, C.G.; Zaninelli, P.G.; Li, L.Z. Assessment of CORDEX simulations over South America: Added value on seasonal climatology and resolution considerations. *Clim. Dyn.* **2019**, *52*, 4771–4786. [[CrossRef](#)]
24. Solman, A.; Blázquez, J. Multiscale precipitation variability over South America: Analysis of the added value of CORDEX RCM simulations. *Clim. Dyn.* **2019**, *53*, 1547–1565. [[CrossRef](#)]
25. Llopard, M.; Reboita, M.S.; da Rocha, R.P. Assessment of multimodel climate projections of water resources over South America CORDEX domain. *Clim. Dyn.* **2020**, *54*, 99–116. [[CrossRef](#)]
26. Spinoni, J.; Barbosa, P.; Bucchignani, E.; Cassano, J.; Cavazos, T.; Christensen, J.H.; Christensen, O.B.; Coppola, E.; Evans, J.; Geyer, B.; et al. Future global meteorological drought hot spots: A study based on CORDEX data. *J. Clim.* **2020**, *33*, 3635–3661. [[CrossRef](#)]
27. Olmo, M.E.; Bettolli, M.L. Extreme daily precipitation in southern South America: Statistical characterization and circulation types using observational datasets and regional climate models. *Clim. Dyn.* **2021**, *57*, 895–916. [[CrossRef](#)]
28. Teichmann, C.; Jacob, D.; Remedio, A.R.; Remke, T.; Buntемeyer, L.; Hoffmann, P.; Kriegsmann, A.; Lierhammer, L.; Bülow, K.; Weber, T.; et al. Assessing mean climate change signals in the global CORDEX-CORE ensemble. *Clim. Dyn.* **2021**, *57*, 1269–1292. [[CrossRef](#)]
29. Ashfaq, M.; Cavazos, T.; Reboita, M.S.; Torres-Alavez, J.A.; Im, E.S.; Olusegun, C.F.; Alves, L.; Kesondra, K.; Adeniyi, M.O.; Moustapha, T.; et al. Robust late twenty-first century shift in the regional monsoons in RegCM-CORDEX simulations. *Clim. Dyn.* **2021**, *57*, 1463–1488. [[CrossRef](#)]
30. Reboita, M.S.; Reale, M.; da Rocha, R.P.; Giorgi, F.; Giuliani, G.; Coppola, E.; Nino, R.B.L.; Llopard, M.; Torres, J.A.; Cavazos, T. Future changes in the wintertime cyclonic activity over the CORDEX-CORE southern hemisphere domains in a multi-model approach. *Clim. Dyn.* **2021**, *57*, 1533–1549. [[CrossRef](#)]
31. Coppola, E.; Raffaele, F.; Giorgi, F.; Giuliani, G.; Xuejie, G.; Ciarlo, J.M.; Sines, T.R.; Torres-Alavez, J.A.; Das, S.; di Sante, F.; et al. Climate hazards indices projections based on CORDEX-CORE, CMIP5 and CMIP6 ensemble. *Clim. Dyn.* **2021**, *57*, 1293–1383. [[CrossRef](#)]
32. Llopard, M.; Domingues, L.M.; Torma, C.; Giorgi, F.; da Rocha, R.P.; Ambrizzi, T.; Reboita, M.S.; Alves, L.M.; Coppola, E.; da Silva, M.L.; et al. Assessing changes in the atmospheric water budget as drivers for precipitation change over two CORDEX-CORE domains. *Clim. Dyn.* **2021**, *57*, 1615–1628. [[CrossRef](#)]
33. Glazer, R.H.; Torres-Alavez, J.A.; Coppola, E.; Giorgi, F.; Das, S.; Ashfaq, M.; Sines, T. Projected changes to Severe thunderstorm environments as a result of twenty-first century warming from RegCM CORDEX-CORE simulations. *Clim. Dyn.* **2021**, *57*, 1595–1613. [[CrossRef](#)]
34. Torres-Alavez, J.A.; Das, S.; Corrales-Suastegui, A.; Coppola, E.; Giorgi, F.; Raffaele, F.; Bukovsky, M.S.; Ashfaq, M.; Salinas, J.A.; Sines, T. Future projections in the Climatology of global low-level jets from CORDEX-CORE simulations. *Clim. Dyn.* **2021**, *57*, 1551–1569. [[CrossRef](#)]
35. Alexander, L.V.; Fowler, H.J.; Bador, M.; Behrangi, A.; Donat, M.G.; Dunn, R.; Funk, C.; Goldie, J.; Lewis, E.; Rogé, M.; et al. On the use of indices to study extreme precipitation on sub-daily and daily timescales. *Environ. Res. Lett.* **2019**, *14*, 125008. [[CrossRef](#)]
36. Klein Tank, A.M.G.; Zwiers, F.W.; Zhang, X. Guidelines on Analysis of Extremes in a Changing Climate in Support of Informed Decisions for Adaptation. WMO-TD/No.1500, WCDMP-72. 2009. Available online: https://library.wmo.int/index.php?lvl=notice_display&id=138 (accessed on 15 July 2022).

37. Zhang, X.; Alexander, L.; Hegerl, G.C.; Jones, P.; Tank, A.K.; Peterson, T.C.; Trewin, B.; Zwiers, F.W. Indices for monitoring changes in extremes based on daily temperature and precipitation data. *Wiley Interdiscip. Rev. Clim. Chang.* **2011**, *2*, 851–870. [CrossRef]
38. Kim, Y.H.; Min, S.K.; Zhang, X.; Sillmann, J.; Sandstad, M. Evaluation of the CMIP6 multi-model ensemble for climate extreme indices. *Weather Clim. Extrem.* **2020**, *29*, 100269. [CrossRef]
39. Statista. Electricity Generation in South and Central America in 2021, by Fuel Type. Available online: <https://www.statista.com/statistics/983336/central-south-america-electricity-generation-source/#:~{:text=In%202021%2C%20hydropower%20dominated%20the,electricity%20generated%20in%20the%20region}> (accessed on 4 August 2022).
40. International Energy Agency. Climate Impacts on Latin American Hydropower. Available online: <https://www.iea.org/reports/climate-impacts-on-latin-american-hydropower/climate-impacts-on-latin-american-hydropower> (accessed on 4 August 2022).
41. BizVibe. Hydropower Generation Industry: Top 20 Hydropower Producing Countries in the World 2020. Available online: <https://blog.bizvibe.com/blog/uncategorized/top-hydropower-producing-countries> (accessed on 4 August 2022).
42. Reboita, M.S.; Gan, M.A.; da Rocha, R.P.; Ambrizzi, T. Regimes de precipitação na América do Sul: Uma revisão bibliográfica. *Rev. Bras. Meteorol.* **2010**, *25*, 185–204. [CrossRef]
43. Ferreira, G.W.S.; Reboita, M.S. A new look into the South America precipitation regimes: Observation and Forecast. *Atmosphere* **2022**, *13*, 873. [CrossRef]
44. Statista. The Ten Largest River Drainage Basins on the Earth as of 2021. Available online: <https://www.statista.com/statistics/1221316/ten-largest-river-basin-worldwide/#:~{:text=As%20of%202021%2C%20the%20Amazon,nearly%20seven%20million%20square%20kilometers}> (accessed on 20 July 2022).
45. Chen, M.; Shi, W.; Xie, P.; Silva, V.B.S.; Kousky, V.E.; Higgins, R.W.; Janowiak, J.E. Assessing objective techniques for gauge-based analyses of global daily precipitation. *J. Geophys. Res.* **2008**, *113*, D04110. [CrossRef]
46. Marraon, V.H.; Reboita, M.S. Características da precipitação na América do Sul reveladas através de índices climáticos. *Rev. Bras. Climatol.* **2020**, *26*, 663–675. [CrossRef]
47. Blázquez, J.; Solman, A. Multiscale precipitation variability and extremes over South America: Analysis of future changes from a set of CORDEX regional climate model simulations. *Clim. Dyn.* **2020**, *55*, 2089–2106. [CrossRef]
48. Balmaceda-Huarte, R.; Olmo, M.E.; Bettolli, M.L.; Poggi, M.M. Evaluation of multiple reanalyses in reproducing the spatio-temporal variability of temperature and precipitation indices over southern South America. *Int. J. Climatol.* **2021**, *41*, 5572–5595. [CrossRef]
49. van Vuuren, D.P.; Edmonds, J.; Kainuma, M.; Riahi, K.; Thomson, A.; Hibbard, K.; Hurtt, G.C.; Kram, T.; Krey, V.; Lamarque, J.-F.; et al. The representative concentration pathways: An overview. *Clim. Chang.* **2011**, *109*, 5. [CrossRef]
50. WMO. WMO Statement on the State of the Global Climate in 2019, WMO-No. 1248. Available online: https://library.wmo.int/doc_num.php?explnum_id=10211 (accessed on 10 July 2022).
51. The Conversation 2020. It's Official: The Last Five Years Were the Warmest Ever Recorded. Available online: <https://theconversation.com/its-official-the-last-five-years-were-the-warmest-ever-recorded-133056> (accessed on 10 July 2022).
52. Mesinger, F.; Chou, S.C.; Gomes, J.L.; Jovic, D.; Bastos, P.; Bustamante, J.F.; Lazic, L.; Lyra, A.A.; Morelli, S.; Ristic, I.; et al. An upgraded version of the Eta model. *Meteorol. Atmos. Phys.* **2012**, *116*, 63–79. [CrossRef]
53. Chylek, P.; Li, J.; Dubey, M.K.; Wang, M.; Lesins, G. Observed and model simulated 20th century Arctic temperature variability: Canadian Earth System Model CanESM2. *Atmos. Chem. Phys. Discuss.* **2011**, *11*, 22893–22907. [CrossRef]
54. Arora, V.K.; Scinocca, J.F.; Boer, G.J.; Christian, J.R.; Denman, K.L.; Flato, G.M.; Kharin, V.V.; Lee, W.G.; Merryfield, W.J. Carbon emission limits required to satisfy future representative concentration pathways of greenhouse gases. *Geophys. Res. Lett.* **2011**, *38*, L05805. [CrossRef]
55. Collins, W.J.; Bellouin, N.; Doutriaux-Boucher, M.; Gedney, N.; Halloran, P.; Hinton, T.; Hughes, J.; Jones, C.D.; Joshi, M.; Liddicoat, S.; et al. Development and evaluation of an Earth-System model—HadGEM2. *Geosci. Model Dev.* **2011**, *4*, 1051–1075. [CrossRef]
56. Martin, G.M.; Bellouin, N.; Collins, W.J.; Culverwell, I.D.; Halloran, P.R.; Hardiman, S.C.; Hinton, T.J.; Jones, C.D.; McDonald, R.E.; McLaren, A.J.; et al. The HadGEM2 family of Met Office unified model climate configurations. *Geosci. Model Dev.* **2011**, *4*, 723–757. [CrossRef]
57. Watanabe, M.; Suzuki, T.; Oishi, R.; Komuro, Y.; Watanabe, S.; Emori, S.; Takemura, T.; Chikira, M.; Ogura, T.; Sekiguchi, M.; et al. Improved climate simulation by MIROC5: Mean states, variability, and climate sensitivity. *J. Clim.* **2010**, *23*, 6312–6335. [CrossRef]
58. Bentsen, M.; Bethke, I.; Debernard, J.B.; Iversen, T.; Kirkevåg, A.; Seland, Ø.; Drange, H.; Roelandt, C.; Seierstad, I.A.; Hoose, C.; et al. The Norwegian Earth System Model, NorESM1-M—Part 1: Description and basic evaluation of the physical climate. *Geosci. Model Dev.* **2013**, *6*, 687–720. [CrossRef]
59. Stevens, B.; Giorgetta, M.; Esch, M.; Mauritsen, T.; Crueger, T.; Rast, S.; Salzmann, M.; Schmidt, H.; Bader, J.; Block, K.; et al. Atmospheric component of the MPI-M Earth System model: ECHAM6. *J. Adv. Model. Earth Syst.* **2013**, *5*, 146–172. [CrossRef]
60. Jacob, D.; Elizalde, A.; Haensler, A.; Hagemann, S.; Kumar, P.; Podzun, R.; Wilhelm, C. Assessing the transferability of the regional climate model REMO to different coordinated regional climate downscaling experiment (CORDEX) regions. *Atmosphere* **2012**, *3*, 181–199. [CrossRef]
61. Peterson, T.C.; Folland, C.; Gruza, G.; Hogg, W.; Mokssit, A.; Plummer, N. *Report on the Activities of the Working Group on Climate Change Detection and Related Rapporteurs*; World Meteorological Organization: Geneva, Switzerland, 2001; Available online: <http://etcdd.pacificclimate.org/docs/wgccd.2001.pdf> (accessed on 8 August 2022).

62. Gilewski, P.; Nawalany, M. Inter-comparison of rain-gauge, radar, and satellite (IMERG GPM) precipitation estimates performance for rainfall-runoff modeling in a mountainous catchment in Poland. *Water* **2018**, *10*, 1665. [[CrossRef](#)]
63. Mann, H.B. Nonparametric tests against trend. *Econometrica* **1945**, *13*, 245–259. [[CrossRef](#)]
64. Kendall, M.G. *Rank Correlation Methods*, 4th ed.; Charles Griffin: London, UK, 1975.
65. Gilbert, R.O. *Statistical Methods for Environmental Pollution Monitoring*; Van Nostrand Reinhold: New York, NY, USA, 1987.
66. Glen, S. Mann Kendall Trend Test: Definition, Running the Test. Available online: <https://www.statisticshowto.com/mann-kendall-trend-test/> (accessed on 15 July 2022).
67. Escobar, G.C.J.; Reboita, M.S. Relationship between daily atmospheric circulation patterns and South Atlantic Convergence Zone (SACZ) events. *Atmósfera* **2022**, *35*, 1–25. [[CrossRef](#)]
68. Díaz, L.B.; Vera, C.S. Austral summer precipitation interannual variability and trends over Southeastern South America in CMIP5 models. *Int. J. Climatol.* **2017**, *37*, 681–695. [[CrossRef](#)]
69. Alves, L.M.; Chadwick, R.; Moise, A.; Brown, J.; Marengo, J.A. Assessment of rainfall variability and future change in Brazil across multiple timescales. *Int. J. Climatol.* **2020**, *41*, E1875–E1888. [[CrossRef](#)]
70. Ortega, G.; Arias, P.A.; Villegas, J.C.; Marquet, P.A.; Nobre, P. Present-day and future climate over central and South America according to CMIP5/CMIP6 models. *Int. J. Climatol.* **2022**, *41*, 6713–6735. [[CrossRef](#)]
71. Bruick, Z.S.; Rasmussen, K.L.; Cecil, D.J. Subtropical South American hailstorm characteristics and environments. *Mon. Weather Rev.* **2019**, *147*, 4289–4304. [[CrossRef](#)]
72. Kousky, V.E. Pentad outgoing longwave radiation climatology for the South American sector. *Rev. Bras. Meteorol.* **1988**, *3*, 217–223.
73. Carvalho, L.M.V.; Jones, C.; Liebmann, B. The South Atlantic Convergence Zone: Intensity, form, persistence, and relationships with intraseasonal to interannual activity and extreme rainfall. *J. Clim.* **2004**, *17*, 88–108. [[CrossRef](#)]
74. Silva, J.P.R.; Reboita, M.S.; Escobar, G.C.J. Caracterização da Zona de Convergência do Atlântico Sul em campos atmosféricos recentes. *Rev. Bras. Climatol.* **2019**, *25*, 355–377. [[CrossRef](#)]
75. Salio, P.; Nicolini, M.; Zipser, E.J. Mesoscale convective systems over southeastern South America and their relationship with the South American low-level jet. *Mon. Weather Rev.* **2007**, *135*, 1290–1309. [[CrossRef](#)]
76. Abdullaev, S.M.; Zhelnin, A.A.; Lenskaya, O.Y. Life cycle of mesoscale convective systems. *Russ. Meteorol. Hydrol.* **2009**, *34*, 285–292. [[CrossRef](#)]
77. Filho, A.; Carbone, R.; Tuttle, J. Convective rainfall systems in the La Plata Basin. *Atmos. Clim. Sci.* **2014**, *4*, 757–778. [[CrossRef](#)]
78. Iacobone, M.F.; Pántano, V.C.; Penalba, O.C. Consecutive dry and wet days over South America and their association with ENSO events, in CMIP5 simulations. *Theor. Appl. Climatol.* **2020**, *142*, 791–804. [[CrossRef](#)]
79. Reboita, M.S.; Ambrizzi, T.; Silva, B.A.; Pinheiro, R.F.; da Rocha, R.P. The South Atlantic subtropical anticyclone: Present and future climate. *Front. Earth Sci.* **2019**, *7*, 8. [[CrossRef](#)]
80. Almazroui, M.; Ashfaq, M.; Islam, M.N.; Kamil, S.; Abid, M.A.; O'Brien, E.; Ismail, M.; Reboita, M.S.; Sörensson, A.A.; Arias, P.A.; et al. Assessment of CMIP6 performance and projected temperature and precipitation changes over South America. *Earth Syst. Environ.* **2021**, *5*, 155–183. [[CrossRef](#)]
81. Reboita, M.S.; Kiani, R.S.; Ali, S.; Khan, T. Projections of wind power density in Pakistan and adjacent regions. *Clim. Res.* **2021**, *85*, 177–192. [[CrossRef](#)]
82. Visser, H.; Folkert, R.J.M.; Hoekstra, J.; De Wolff, J.J. Identifying key sources of uncertainty in climate change projections. *Clim. Chang.* **2000**, *45*, 421–457. [[CrossRef](#)]
83. Giorgi, F. Uncertainties in climate change projections, from the global to the regional scale. *EPJ Web Conf.* **2010**, *9*, 115–129. [[CrossRef](#)]
84. Latif, M. Uncertainty in climate change projections. *J. Geochem. Explor.* **2011**, *110*, 1–7. [[CrossRef](#)]
85. Deser, C.; Phillips, A.; Bourdette, V.; Teng, H. Uncertainty in climate change projections: The role of internal variability. *Clim. Dyn.* **2012**, *38*, 527–546. [[CrossRef](#)]
86. Mehta, L.; Adam, H.N.; Srivastava, S. Unpacking uncertainty and climate change from ‘above’ and ‘below’. *Reg. Environ. Chang.* **2019**, *19*, 1529–1532. [[CrossRef](#)]
87. Scientific uncertainty. *Nat. Clim. Chang.* **2019**, *9*, 797. [[CrossRef](#)]
88. Zandonadi, L.; Acquaotta, F.; Fratianni, S.; Zavattini, J.A. Changes in precipitation extremes in Brazil (Paraná River Basin). *Theor. Appl. Climatol.* **2016**, *123*, 741–756. [[CrossRef](#)]
89. Soares, D.; Lee, H.; Loikith, P.; Barkhordarian, A.; Mechoso, C. Can significant trends be detected in surface air temperature and precipitation over South America in recent decades? *Int. J. Climatol.* **2017**, *37*, 1483–1493. [[CrossRef](#)]
90. Cerón, W.L.; Kayano, M.T.; Andreoli, R.V.; Avila-Diaz, A.; Ayes, I.; Freitas, E.D.; Souza, R.A. Recent intensification of extreme precipitation events in the La Plata Basin in Southern South America (1981–2018). *Atmos. Res.* **2021**, *249*, 105299. [[CrossRef](#)]
91. Marengo, J.A.; Ambrizzi, T.; Alves, L.M.; Barreto, N.J.C.; Reboita, M.S.; Ramos, A.M. Changing trends in rainfall extremes in the metropolitan area of São Paulo: Causes and impacts. *Front. Clim.* **2020**, *2*, 3. [[CrossRef](#)]
92. Robertson, A.; Mechoso, C.R. Interannual and interdecadal variability of the South Atlantic convergence zone. *Mon. Weather Rev.* **2000**, *128*, 2947–2957. [[CrossRef](#)]
93. Mo, K.C.; Nogués-Paegle, J. The Pacific-South American modes and their downstream effects. *Int. J. Climatol.* **2001**, *21*, 1211–1229. [[CrossRef](#)]

94. Skansi, M.; Brunet, M.; Sigró, J.; Aguilar, E.; Groening, J.A.A.; Bentancur, O.J.; Jones, P.D. Warming and wetting signals emerging from analysis of changes in climate extreme indices over South America. *Glob. Planet. Chang.* **2013**, *100*, 295–307. [CrossRef]
95. WMO. State of the Global Climate 2021, WMO-No. 1290. Available online: https://library.wmo.int/doc_num.php?explnum_id=11178 (accessed on 1 July 2022).
96. BBC. Petrópolis: Deadly Landslides Wreak Havoc in Brazilian City. Available online: <https://www.bbc.com/news/world-latin-america-60401611> (accessed on 1 July 2022).
97. CNN. Com Mais de 530 Milímetros, Petrópolis Registra Maior Chuva da História. Available online: <https://www.cnnbrasil.com.br/nacional/com-mais-de-530-milimetros-petropolis-registra-maior-chuva-da-historia/#:~{:text=O%20n%C3%BAmero%20foi%20superior%20ao,e%20quatro%20pessoas%20seguem%20desaparecidas}> (accessed on 1 July 2022).
98. Floodlist. Brazil—Deadly Floods and Landslides Strike Again in Petrópolis. Available online: <https://floodlist.com/america/brazil-floods-landslides-petropolis-march-2022> (accessed on 1 July 2022).
99. Fischer, E.M.; Sippel, S.; Knutti, R. Increasing probability of record-shattering climate extremes. *Nat. Clim. Chang.* **2021**, *11*, 689–695. [CrossRef]
100. Poder360. Chuvas em Petrópolis já Mataram 238 Pessoas em 2022. Available online: <https://www.poder360.com.br/brasil/chuvas-em-petropolis-ja-mataram-233-pessoas-em-2022/> (accessed on 1 July 2022).
101. National Academies of Sciences, Engineering, and Medicine. *Attribution of Extreme Weather Events in the Context of Climate Change*, 1st ed.; The National Academies Press: Washington, DC, USA, 2016; 186p. [CrossRef]
102. Clarke, B.; Otto, F.; Stuart-Smith, R.; Harrington, L. Extreme weather impacts of climate change: An attribution perspective. *Environ. Res. Clim.* **2022**, *1*, 012001. [CrossRef]
103. Reboita, M.S.; Ambrizzi, T. Climate system in a nutshell: An overview for understanding climate change. *Int. J. Dev. Res.* **2022**, *12*, 53365–53378. [CrossRef]
104. Kjellsson, J. Weakening of the global atmospheric circulation with global warming. *Clim. Dyn.* **2014**, *45*, 975–988. [CrossRef]
105. Pfahl, S.; O’Gorman, P.A.; Fischer, E.M. Understanding the regional pattern of projected future changes in extreme precipitation. *Nat. Clim. Chang.* **2017**, *7*, 423–427. [CrossRef]
106. Chai, Y.; Yue, Y.; Slater, L.J.; Yin, J.; Borthwick, A.G.L.; Chen, T.; Wang, G. Constrained CMIP6 projections indicate less warming and a slower increase in water availability across Asia. *Nat. Commun.* **2022**, *13*, 4124. [CrossRef]
107. Weart, S. The Discovery of Global Warming: Timeline. Available online: <https://history.aip.org/climate/timeline.htm#:~{:text=Mean%20global%20temperature%20}> (accessed on 17 June 2022).
108. Robinson, A.; Lehmann, J.; Barriopedro, D.; Rahmstorf, S.; Coumou, D. Increasing heat and rainfall extremes now far outside the historical climate. *NPJ Clim. Atmos. Sci.* **2021**, *4*, 45. [CrossRef]
109. BBC. Extreme Weather: What Is It and How Is It Connected to Climate Change? Available online: <https://www.bbc.com/news/science-environment-58073295> (accessed on 17 June 2022).
110. APNews. UK Breaks Record for Highest Temperature as Europe Sizzles. Available online: <https://apnews.com/article/wildfires-france-fires-london-england-b9bc07c1685b76ddf377b65f19fb811b> (accessed on 15 July 2022).
111. de Jesus, E.M.; da Rocha, R.P.; Crespo, N.M.; Reboita, M.S.; Gozzo, L.F. Multi-model climate projections of the main cyclogenesis hot-spots and associated winds over the eastern coast of South America. *Clim. Dyn.* **2021**, *56*, 537–557. [CrossRef]
112. Ainsworth, E.A.; Rogers, A. The response of photosynthesis and stomatal conductance to rising [CO₂]: Mechanisms and environmental interactions. *Plant Cell Environ.* **2007**, *30*, 258–270. [CrossRef]
113. Jarvis, A.J.; Mansfield, T.A.; Davies, W.J. Stomatal behaviour, photosynthesis and transpiration under rising CO₂. *Plant Cell Environ.* **1999**, *22*, 639–648. [CrossRef]
114. Zeppel, M.J.B.; Lewis, J.D.; Chaszar, B.; Smith, R.A.; Medlyn, B.E.; Huxman, T.E.; Tissue, D.T. Nocturnal stomatal conductance responses to rising [CO₂], temperature and drought. *New Phytol.* **2012**, *193*, 929–938. [CrossRef]
115. Lyu, K.; Zhang, X.; Church, J.A. Regional dynamic sea level simulated in the CMIP5 and CMIP6 models: Mean biases, future projections, and their linkages. *J. Clim.* **2020**, *33*, 6377–6398. [CrossRef]